Feature Article

Hydroxyl Radical Recycling in Isoprene Oxidation Driven by Hydrogen Bonding and Hydrogen Tunneling: the Upgraded LIM1 Mechanism

Jozef Peeters, Jean-Francois J. Müller, Trissevgeni Stavrakou, and Vinh Son Nguyen

J. Phys. Chem. A, **Just Accepted Manuscript** • DOI: 10.1021/jp5033146 • Publication Date (Web): 10 Jul 2014

Hydroxyl Radical Recycling in Isoprene Oxidation Driven by Hydrogen Bonding and Hydrogen Tunneling: the Upgraded LIM1 Mechanism

Jozef Peeters,[1]* Jean-François Müller,[2] Trissevgeni Stavrakou,[2] and Vinh Son Nguyen[1]

[1] Department of Chemistry, University of Leuven, B-3001 Heverlee, Belgium

[2] Belgian Institute for Space Aeronomy, Avenue Circulaire 3, B-1180 Brussels, Belgium

***jozef.peeters@chem.kuleuven.be**

Abstract

The Leuven Isoprene Mechanism, proposed earlier to aid in rationalizing the unexpectedly high hydroxyl radical (OH) concentrations in isoprene-rich, low-nitric-oxide (NO) regions (Peeters et al. *Phys. Chem. Chem. Phys*. **2009**, 11, 5935), is presented in an upgraded and extended version, LIM1. The kinetics of the crucial reactions in the proposed isoprene-peroxy radical interconversion and isomerisation pathways are re-evaluated theoretically, based on energy barriers computed at the much higher CCSD(T)/aug-cc-pVTZ//QCISD/6-311G(d,p) level of theory, and using multi-conformer partition functions obtained at the M06-2X/6-311++G(3df,2p) level that, different from the B3LYP level used in our earlier work, accounts for the crucial London dispersion effects in the H-bonded systems involved. The steady-state fraction of the specific *Z*-δ-OH-peroxy radical isomers/conformers that can isomerise by 1,6-H shift is shown to be

largely governed by hydrogen-bond strengths, while their isomerisation itself is found to occur quasi-exclusively by hydrogen atom tunneling. The isomer-specific *Z*-δ-OH-peroxy 1,6-H shift rate coefficients are predicted to be of the order of 1 s^{-1} at 298 K, but the experimentally accessible bulk rate coefficients, which have to be clearly distinguished from the former, are two orders of magnitude lower due to the very low *Z*-δ-OH-peroxy steady-state fractions that are only around or below 0.01 at low to moderate NO and depend on the peroxy lifetime. Two pathways subsequent to the peroxy radical 1,6-H shift are identified, the earlier predicted route yielding the photolabile hydroperoxy-methyl-butenals (HPALDs), and a second, about equally important path, to di-hydroperoxy-carbonyl peroxy radicals (di-HPCARP). Taking this into account, our predicted bulk peroxy isomerisation rate coefficients are about a factor 1.8 higher than the available experimental results for HPALD production (Crounse et al. *Phys. Chem. Chem. Phys.* **2011**, 13, 13607), which is within the respective uncertainty margins. We also show that the experimental temperature dependence of the HPALD production rates as well as the observed kinetic isotope effect for per-deuterated isoprene support quantitatively our theoretical peroxy interconversion rates. Global modeling implementing LIM1 indicates that on average about 28% of the isoprene peroxys react via the 1,6-H shift isomerisation route, representing 100 - 150 Tg carbon per year. The fast photolysis of HPALDs we proposed earlier as primary OH regeneration mechanism (Peeters and Muller, *Phys. Chem. Chem. Phys*. **2010**, 12, 14227) found already experimental confirmation (Wolfe et al. *Phys. Chem. Chem. Phys.* **2012**, 14, 7276); based on further theoretical work in progress, reaction schemes are presented of the oxy co-product radicals from HPALD photolysis and of the di-HPCARP radicals from the

second pathway following peroxy isomerisation that are both expected to initiate considerable additional OH recycling.

Keywords: Atmospheric chemistry; isoprene; hydroxyl radicals, chemical mechanisms, peroxy radicals, isomerisations.

Introduction

Biogenic emissions by vegetation are responsible for 90% of the volatile organic compounds (VOC) in our atmosphere.[1,2] Isoprene (CH_2=C(CH_3)-CH=CH_2), with global emissions of about 500 Tg per year, is by far the most abundant of the biogenic compounds, accounting for about half of the total.[3] As its emissions are light- and temperature-controlled, the highest emission rates are from forests in and near the tropics, coinciding with high production rates of the major atmospheric oxidant, the hydroxyl radical (OH), which is formed mainly by photolysis of ozone (O_3) and reaction of the resulting excited oxygen (O) atoms with water vapor. The atmospheric oxidation of isoprene is initiated predominantly by its fast reaction with OH, a process that influences the OH concentration and thereby also the atmospheric lifetime of pollutants such as carbon monoxide (CO) and of greenhouse gases such as methane. In the presence of sufficiently high concentrations of nitric oxide (NO), the hydroxy-peroxy radicals ($ISOPO_2$) from the initial reaction of isoprene with OH react with NO to form HO_2 radicals that react in turn with NO to regenerate OH and form nitrogen dioxide (NO_2), which subsequently photolyses to NO and ground state O atoms that combine with O_2 to produce ozone. However, at low NO, the $ISOPO_2$ radicals will react for the larger part with HO_2 radicals to produce hydroperoxides, which in turn react with OH in an OH-

neutral reaction to yield isoprene epoxides,[4] thought to be one of the precursors of the secondary organic aerosol that is formed in great abundance from isoprene — by which isoprene also affects climate.[5,6] As a result, it was generally considered that at low NO levels, isoprene would strongly deplete OH radicals. However, in several field campaigns during the past 15 years in isoprene-rich areas, among others in the Amazon basin, the Pearl River Delta, and Borneo, unexpectedly high OH concentrations were measured, up to 10 times more than predicted by current models, and with $[OH]_{obs}/[OH]_{mod}$ ratios often correlating well with the isoprene mixing ratio, strongly indicating fast OH recycling in isoprene oxidation.[7,8,9,10,11,12,13,14,15,16,17,18] Even though part of the high measured [OH] might be due to instrumental artifacts, as reported by Mao et al.,[19] the underlying possible mechanisms are a major current topic in atmospheric chemistry.

In a series of proof-of-concept papers, we recently proposed novel peroxy radical pathways in isoprene oxidation at low and moderate NO levels, aiming to rationalize the observed OH regeneration, at least for a part, by viable chemical mechanisms.[20,21,22] The key new features in the preliminary version of the Leuven Isoprene Mechanism (LIM), shown also in Figures 1 and 2, are : (i) fast redissociation and interconversion to near-equilibration at low NO-levels of the thermally labile, allylic δ-hydroxy- and β-hydroxy-isoprenylperoxy radicals; (ii) rapid isomerisation of the *Z*-δ-OH-isoprenylperoxy radicals by 1,6-H shifts leading to HO_2 radicals and photolabile hydroperoxy-methyl-butenals (HPALDs); (iii) OH regeneration via very fast photolysis of the HPALDs and subsequent chemistry; and (iv) direct recycling of OH by isomerisation and decomposition of the β-OH-isoprenylperoxys *via* concerted 1,5-H shift, suggested also by da Silva.[23] In these first papers, above, order-of-magnitude estimates were made of the pertaining re-

dissociation and isomerisation rates at low-to-moderate levels of quantum-chemical and statistical-rate theories, and the potential major impact of this preliminarily LIM mechanism on the [OH] and [HO_2] concentrations was demonstrated by global modelling.[24,25,26]

Meanwhile, substantial HPALD formation in isoprene oxidation has been observed in the laboratory by Crounse et al.,[27] although at yields considerably lower than our predicted *total* products yield from the 1,6-H shift, but no evidence was found for the unimolecular production of methylvinylketone (MVK) and methacrolein (MACR) expected from the concerted 1,5-H shifts of the β-OH-isoprenylperoxys. Moreover, Wolfe et al.[28] have confirmed experimentally the unusually fast photolysis of HPALDs to form OH with near-unit quantum yield as predicted. Very recently, Fuchs et al. reported the direct observation of about 60% OH regeneration in isoprene oxidation under controlled atmospheric conditions (NO levels about 100 pptv) in their atmospheric simulation chamber, finding their results consistent with the postulated unimolecular reactions of isoprene-derived peroxy radicals, above.[18] Although these authors consider that the observed OH recycling is not sufficient to explain the very high concentrations of hydroxyl radicals observed in some field campaigns, they conclude that it contributes significantly to the oxidizing capacity of the atmosphere in isoprene-rich regions.

Well aware that our preliminary kinetic quantification of the new mechanistic features proposed in LIM0 was based on quantum chemical data at (too) low levels of theory, and that the further chemistry following the peroxy radical isomerisations, including the precise mechanism of HPALD photolysis, needed to be examined much more closely, we have, the past few years, greatly upgraded and further extended these mechanisms and

their kinetics, bringing to bear the highest feasible levels of *ab initio* and DFT theories we can currently apply to the fairly large molecules of interest.

In this article, the upgraded and expanded LIM1 mechanism will be detailed and the much more reliable kinetic data resulting from the higher-level theoretical treatments will be presented at some length. The contributions or yields of the novel pathways predicted on basis of the new kinetic data will be confronted with the available experimental results via box modelling. We will also briefly outline the follow-up chemistries of the HPALD photolysis co-product and of a parallel novel reaction pathway — for which experimental evidence is also available — as they emerge from ongoing further theoretical work.

Methodologies

Theoretical studies of OH-initiated oxidation mechanism of isoprene

The methodology of choice for the theoretical development of the isoprene oxidation mechanism is 1° high-level quantum-chemical characterisation and 2° subsequent theoretical-kinetics quantification of reactions that are expected to be significant according to new insights and/or for which indications have been provided by novel experimental results. Such methodologies have been applied by us during the past 15 years, among others for the construction of the oxidation mechanisms of α-pinene[29,30] incorporated in the BOREAM model,[31,32] and allowed the identification and quantification of a number of non-traditional reactions of substituted alkoxy and peroxy radicals in the oxidation of larger biogenic compounds,[33,34,35] with the novel isoprene hydroxy-peroxy radical isomerisations at issue as a prime example.[20]

In this work, much higher-quality quantum chemical DFT and *ab initio* methods are brought to bear. The new-generation, powerful DFT functional M06-2X[36] with large 6-311++G(3df,2p) basis set,[37,38] further designated simply as M06-2X, is used for potential energy surface (PES) constructions. This functional is far superior to B3LYP used in our earlier studies,[20] as, among others, M06-2X accounts properly for the London dispersion effects that are found to be often of critical importance in the hydrogen-bonded structures of interest here. Besides for geometry optimisations, M06-2X is used to calculate multi-conformer partition functions. For crucial, rate-determining reaction steps, geometries of the lowest-energy conformers of reactants and transition states (TS) are optimised using the proven Quadratic Configuration Interaction method, QCISD/6-311G(d,p),[39] and single-point energies are computed using the high-performance but costly Coupled Cluster method with very large basis set, CCSD(T)/aug-cc-PVTZ.[40,41,42] This combination, which we further denote simply as CC//QC, is the most accurate method presently feasible with our facilities for the large molecules of interest. All these calculations were carried out with the Gaussian 09 program suite[43] and Molpro 2012.1 program.[44]

On basis of the quantum computations, advanced theoretical kinetics calculations are performed to obtain temperature- (and pressure-) dependent rate coefficients and branching ratios, using mainly Multi-Conformer Transition State Theory (MC-TST), or RRKM theory and Exact Stochastic Model- based Master Equation analysis for chemically activated reactions. In the MC-TST approach,[45] applied here among others for the key 1,6-H shift isomerisations of the *Z*-δ-OH-isoprenyl-peroxy radicals, all local potential energy minima of a reactant or transition state (TS) separated by high enough

conformational (internal rotation) barriers, of >2 kcal/mol at 300 K, are considered as separate "states", each contributing to the total partition function weighted by the Boltzmann factor $\exp(-\varepsilon_i/k_B T)$. For the crucial peroxy radicals of interest (the *Z*-δ-OH-isoprenyl- and β-OH-isoprenylperoxys), some 20 to 29 relevant conformers are found, and 5 to 7 for the transition states. M06-2X is used for the geometry optimisations of the conformers and for computing their relative energies ε_i with respect to the lowest-lying conformer, as well as for all the data needed to evaluate their partition functions, i.e. vibration frequencies, rotation parameters, and zero-point vibration energies (ZPVE). Note that all relative energies or barrier heights mentioned in the article always include the Δ(ZPVE). It is important to note already here that the presently obtained multi-conformer partition functions and their ratios, at the superior M06-2X level, differ in many instances considerably, often by a factor of 3 to 7, from our earlier results at the lower B3LYP level,[20] mainly because the latter does not take into account London dispersion effects, which are crucial for the H-bonded structures at hand. Tunneling factors for the crucial H shifts in isoprene-derived peroxys are calculated in the asymmetric Eckart-barrier approximation, which was recently shown by Zhang and Dibble to quite well match the high-level small curvature tunneling (SCT) factors calculated for 1,4- and 1,5-H shifts in *n*-pentylperoxy radicals for temperatures around 300 K.[46]

As a second major predictive tool, quantitative Structure-Activity Relationships (SARs) are applied, several of which have been developed or generalized by us, such as SARs for site-specific OH-addition to (poly)alkenes, decomposition of substituted alkoxy radicals, and H-shifts in such radicals.[47,48,49,50]

Theoretical quantification of kinetics of the reactions of the hydroxy-isoprenylperoxy radicals proposed in LIM: Results and Discussion

Figures 1 and 2, which will serve as guides throughout this article, present an overview of all formation and removal reactions of the hydroxy-isoprenylperoxy radicals to be considered in atmospheric conditions at low NO-levels and that determine the concentration fractions of the specific peroxy-isomers that undergo the newly proposed unimolecular reactions. The contributions of these unimolecular reactions to overall isoprene chemistry depend on the fractional populations of these specific isomers as well as on their isomer-specific rates. The peroxy radicals are formed by addition of hydroxyl radicals to isoprene, followed by addition of O_2 to these initial OH-adducts. OH radicals can add to each of the four unsaturated C-atoms of isoprene, labeled as shown below:

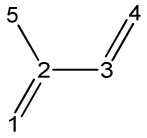

Owing to the conjugated diene structure of isoprene, the initial OH-adducts to the two terminal carbons, denoted in Figures 1 and 2 as OH-Adduct I and OH-Adduct II are resonance-stabilised allylic radicals, e.g. for the OH-Adducts I:

$$HOCH_2\text{-}C^{\bullet}(CH_3)\text{-}CH{=}CH_2 \leftrightarrow HOCH_2\text{-}C(CH_3){=}CH\text{-}CH_2^{\bullet}$$

which also explains why they dominate by far over the much less stable OH-adducts to the two central carbons.[47,51,52] It also follows that O_2 can add to both the major OH-adducts either in β- or in δ- position, resulting in β-OH-isoprenylperoxys and in *Z*- as well as *E*-δ-OH-isoprenylperoxys. The peroxys resulting from OH-Adduct I and OH-Adduct II and their subsequent chemistry are displayed separately in Figures 1 and 2,

respectively. The three peroxy isomers for each case are denoted in these Figures and below as β-OH-peroxy, *Z*-OH-peroxy and *E*-OH-peroxy (followed by I or II when necessary).

Of much consequence, the allyl-resonance stabilisation of 12 - 14 kcal mol^{-1} of the initial OH-Adducts I and II is lost upon O_2-addition, such that the stability of the resulting allylperoxys is expected to be only of the order of 20 kcal/mol, instead of the 30 - 35 kcal/mol for regular alkylperoxys.[53] For this reason, the β-OH- and δ-OH-peroxys from isoprene are thermally unstable at tropospheric temperatures, and their redissociation — and subsequent O_2-readdition — must therefore be expected when the peroxy lifetime is long enough, as in near-pristine low-NO environments, such that the β-OH- and δ-OH-peroxys may actually interconvert and even tend to a thermal equilibrium ratio.[20] Other peroxy removal reactions that likewise determine the population fractions of specific peroxy isomers are the proposed unimolecular H-migration reactions that are central to this paper, also displayed in Figures 1 and 2. Obviously, one needs also to consider the well-known "traditional" peroxy radical reactions with NO and with HO_2 and RO_2 radicals.[54,55] For the reactions of the isoprene-derived peroxys with NO, a rate coefficient $k_{NO} = 9 \times 10^{-12}$ cm^3 s^{-1} at 298 K is generally adopted as for regular alkylperoxys; the products are mainly NO_2 together with the corresponding oxy radicals, $RO_2 + NO \rightarrow RO + NO_2$, the RO giving rise to the bulk of the 1st-generation isoprene oxidation products at high NO levels (see below), but also about 8.5% nitrates, $RO_2 + NO \rightarrow RONO_2$.[54] The reactions of the isoprene peroxys with HO_2, with measured overall rate coefficient $k_{HO2} = 1.7\ 10^{-11}$ cm^3 s^{-1} at 298 K,[56] are believed to produce mainly hydroperoxides, $RO_2 + HO_2 \rightarrow ROOH + O_2$, but recent results indicate also some 6 to 12% formation of $O_2 + OH +$

RO.[4,57] Mutual or cross reactions of the isoprene-peroxys, with weighted average rate coefficient around $k_{HO2} \approx 2 \times 10^{-12}$ cm^3 s^{-1} [58,59] are generally thought to be minor under atmospheric conditions. The total pseudo-first order isoprene-peroxy removal rate by the three traditional reactions combined in pristine or remote regions is mostly in the range of k_{tr} = 0.02 to 0.05 s^{-1}. The rates of the other peroxy removal and interconversion reactions, above, and, in first place, their formation reactions will be addressed in the following subsections.

Addition of OH to isoprene

Four OH-adducts can be formed, including for about 7% OH-adducts to the two inner carbons atoms[60] of which the chemistry is not considered further in this work, and 93 % adducts to the two outer carbons: OH-Adduct I and OH-Adduct II (see Figure 1 and 2). For the latter two, following and concurring with Park et al.,[522] we adopt branching fractions of 62 % and 31%, respectively, to best reproduce the well-established experimental product distribution at high NO as we detail in Section S1 and Table S1. These values are compatible with and close to the averages of two independent theoretical approaches within their expected uncertainties of several %.[47,51,61] Both the OH-Adducts I and II can be formed as either *cis*- or *trans*- allylic structures: their high initial internal energies of some 36 - 39 kcal mol^{-1}, which includes a few kcal mol^{-1} thermal energy, allow for prompt *cis-trans* interconversion, over barriers computed to be only 14-15 kcal mol^{-1},[20] before they are fully collisionally stabilized. An RRKM-master equation analysis revealed that OH-Adducts I collisionally stabilize as ≈ 50% *trans* and ≈ 50% *cis*, whereas the OH-Adducts II end up as ≈ 30% *trans*- and 70% *cis*-OH-Adducts II (see Figures 1 and 2),[20] in excellent agreement with earlier predictions by Dibble.[62] The

addition of O_2 in β position to the OH-Adducts I and II allows for near-free internal rotation of the -CH=CH_2 or -C(CH_3)=CH_2 moieties in the β peroxys, merging the contributions from *cis*- and *trans*- OH-isoprene radicals; however, O_2-addition to the δ-carbon leads to distinct *E*- or *Z*- substituted alkene frames (see Figures 1 and 2).

It must be stressed at this point that the β-OH- ⇌ δ-OH-peroxy interconversion above does not occur between peroxys from different initial OH-adducts. The peroxy pool from the OH-Adducts I remains strictly separated from the pool derived from OH-Adducts II since the initial OH-adducts are far too stable to redissociate. For the peroxy chemistries and subsequent processes, we therefore consider below always two distinct cases: Case I for the chemistry resulting from the OH-Adducts I (Figure 1); and Case II for that from the OH-Adducts II (Figure 2).

Addition of O_2 to hydroxy-isoprene adducts: rate and initial branching ratios

The rate coefficients for the various site-specific O_2-additions, leading to the six different peroxys (see Figures 1 and 2), are obtained from the overall O_2-addition rate k_{+O2}^{bulk}, in combination with the branching to the OH-adducts, above, and with the 1st-generation oxidation-product distribution as measured in laboratory experiments at very high NO, on which there is a consensus within a few percent.[52,63] At very high NO, the various isoprene peroxys react immediately with NO, producing MVK, MACR, CH_2O and unsaturated hydroxy-carbonyls via mechanisms that are well understood. In this way, the relative formation rates of the six isoprene peroxys of interest can be retrieved with good precision. The values adopted in this article differ somewhat from these reported in our earlier seminal paper,[20] because the expected products from the minor, central adducts are now included in the analysis, which is detailed in Section S1 (Supporting

Information, SI). Remarkably, the overall k_{+O2}^{bulk} is not well known. In our earlier paper we used the value of 2.3×10^{-12} cm^3 s^{-1} reported by Park et al., though with a large uncertainty of $\pm 2 \times 10^{-12}$ cm^3 s^{-1}.[52] However, in this work, we have adopted the more recent value of $(1.0 +1.7/-0.5) \times 10^{-12}$ cm^3 s^{-1} determined by Ghosh et al.[64] for O_2 addition to the major OH-Adduct I, a value that lies within the range $(0.7 \pm 0.3) \times 10^{-12}$ cm^3 s^{-1} determined from non-isomer-selective experimental studies performed by Zhang et al.[65] and also within the range of (0.6 to to 2.0) $\times 10^{-12}$ cm^3 s^{-1} determined by Koch et al.[66] at 345 and 300 K, while it is still consistent with the range $(2.3 \pm 2.0) \times 10^{-12}$ cm^3 s^{-1} of the above mentioned study of Park et al.[52] Both the latter studies relied on non-isomer-selective cycling experiments. Quite importantly, as discussed in following sections and shown in Fig. S4, it turns out that at low NO (< 100 ppt) the product distribution deriving from OH-Adduct I shows little sensitivity to k_{+O2}^{bulk}, while it affects the product yields from OH-Adduct II only in a minor way. The rate coefficients derived in this way for the isomer- specific O_2-addition rates k_{+O2} are shown on Figures 1 and 2 and listed also in Table S5. They are all considered independent of temperature, except these leading to the non-hydrogen-bonded *E*-δ-OH-peroxy isomers for which we earlier found a small barrier in the entrance channel.[20] Note that the precise initial branching to the *E*-δ-OH-peroxys is of only marginal importance for this work, since under the low-NO conditions of interest, these isomers are shown below to be in near-equilibrium with the majority β-OH-peroxy isomers anyway.

Redissociation and interconversion of the OH-isoprenylperoxy radicals

To quantify the fractions of the six allylic peroxys, in low-NO conditions, the required rates of their redissociation by O_2 loss, k_{-O2} , can now be evaluated from the k_{+O2} above

via the thermal equilibrium constants, $K_{eq} = k_{+O2} / k_{-O2}$. In this context, it should be noted that, contrary to a suggested "double activation" effect,[67] the OH-Adducts should be fully thermalized when adding O_2, since they will have suffered some 1000 collisions before that. The K_{eq} are evaluated theoretically using a multi-conformer quantum-statistical approach:

$$K_{eq} = \frac{\sum Q_{peroxy}}{Q_{O_2} \times \sum Q_{OH\text{-}Adduct}} \times e^{-\frac{\Delta E}{k_B T}} \qquad (1)$$

in which Q_{O2} is the partition function of O_2; $\sum Q_{peroxy}$ and $\sum Q_{OH\text{-}Adduct}$ are the multi-conformer partition function of the considered peroxy isomer and OH-Adduct isomer, respectively; ΔE is the energy difference between the lowest-energy conformers of peroxy and OH-Adduct + O_2; and k_B is the Boltzmann constant. The relative energies of the lowest-lying conformers of the key β-OH- and *Z*-δ-OH-peroxys and of their OH-Adduct precursors, needed for the critical energy difference ΔE in the exponent of equation (1), were computed at the high-performance CC//QC level of theory. It should be noted that to reduce the computational cost by a factor of ≈10, the CC//QC energies for the lowest conformer were computed for each structure involved (molecule, radical or transition state) with the methyl substituent replaced by an H atom, and including separately the effect of the methyl substituent computed for each structure at the M06-2X level. It was duly verified for a few structures that the accuracy loss of this procedure was only ≈0.15 kcal mol^{-1}. The energy separations ε_i of the various conformers relative to the lowest, and all other parameters required for the multi-conformer partition functions were computed at the M06-2X level (see Methodologies). For each of the crucial β-OH- and *Z*-δ-OH-peroxy radicals of interest, about 25 relevant conformers had to be taken into

account, *versus* 4 to 5 for the allylic OH-Adducts; their relative energies are depicted in Fig. S2. For the less important *trans*-OH-adducts and the *E*-δ-OH-peroxys the ΔE were computed at the M06-2X level. The energies of the lowest-lying conformers of all structures involved for Case I and Case II, together with the geometries, are displayed in Table S2. In each of the two peroxy pools, the β-OH-peroxy isomers are the most stable, mainly because of the 4 to 5 kcal mol^{-1} strong internal hydrogen bond, while the *Z*-δ-OH-peroxy isomers which feature an only weak H-bond, are less stable by 2.22 (Case I) and 2.54 (Case II) kcal mol^{-1} (see Table S2, showing the lowest conformers of each structure of interest); worth noting, these crucial CC//QC computed differences are supported by the M06-2X values being both only 0.19 kcal mol^{-1} higher. The less important *E*-δ-OH-peroxys, lacking an H-bond, are highest in energy but are looser and therefore have somewhat higher partition functions. The CC//QC computed O_2-addition energies ΔE for the various reactions of interest, which can be obtained from these data and are listed as such in Table S2, are only about 20 to 24 kcal mol^{-1} as expected, and therefore low enough for substantial re-dissociation of the peroxys. The K_{eq} values over the temperature range of interest are listed in Table S3.

The *T*-dependent expressions $k_{-O2}(T)$ derived as outlined above, together with the corresponding K_{eq} are listed in Table S5. The k_{-O2} (298 K) values, shown on Figures 1 and 2, are in the range of 0.02 to 5 s^{-1}, which is indeed higher than or at least comparable to the rates $k_{tr} \approx 0.02$ to 0.05 s^{-1} of their irreversible removal by $NO/HO_2/RO_2$ in near-pristine, isoprene-rich areas. The highest redissociation rates are found for the *Z*- and *E*-δ-OH-peroxys, in particular for Case I, with k_{-O2} (298 K) approaching 5 s^{-1}. Both the *E*- and *Z*-δ-OH-peroxy isomers in each separate pool (Case I; Case II) may then tend to

thermal equilibration with the majority β-OH-peroxys, but, as made clear in a next subsection, full equilibration, within 5%, of

β-OH-peroxy ⇌ *Z*-δ-OH-peroxy (Ra)

is only possible for the Case I peroxys, and then only at temperatures $T \geq 310$K, while for the Case II peroxys, these equilibria are far from attained. Still, the $K_{eq}(T)$ for these indirect, potential equilibria are of interest here; the values over the temperature range of interest are also listed in Table S3 and the $K_{eq}(T)$ expressions are given in Table S5. Abbreviating $K_{eq\ a} \equiv \{[Z\text{-}\delta]/[\beta]\}_{eq}$ for potential equilibrium (Ra) as $K_{eq}(Z\text{-}\delta/\beta)$, and $K_{eq\ b} \equiv \{[E\text{-}\delta]/[\beta]\}_{eq}$ for potential equilibrium

β-OH-peroxy ⇌ *E*-δ-OH-peroxy (Rb)

as $K_{eq}(E\text{-}\delta/\beta)$, we find for Case I: $K_{eq}(Z\text{-}\delta/\beta)(I) = 0.0133$ and $K_{eq}(E\text{-}\delta/\beta)(I) = 0.0158$ at 298 K, such that the β-OH-peroxys would make up ≥ 97% of a potential peroxy equilibrium population. The K_{eq} data for the Case II peroxys are quite similar, but the actual steady-state $\{[Z\text{-}\delta]/[\beta]\}$ ratio at low NO is far below the equilibrium value.

It can be noted that the present $\{[Z\text{-}\delta]/[\beta]\}_{eq}$values, computed at high levels of theory, are about 4 times lower than the preliminary values of about 0.06 in our earlier proof-of-concept communication.[20] The major reason is that the multi-conformer partition function ratio of the *Z*-δ-OH- and β-OH-peroxy isomers computed presently at the superior M06-2X level is much lower than obtained earlier with the lower-level B3LYP functional that neglects London dispersion and hence substantially underestimates several low-vibration frequencies of the *Z*-δ-OH- peroxy conformers and moreover predicts too small energy separations between the lower *Z*- δ-OH-peroxy conformers.

In a very recent paper,[68] the k_{-O2} of the *Z*-δ-OH-peroxys and the total k_{-O2} of the β-OH-peroxys for Case I were theoretically derived directly — a notoriously difficult task for impulsive dissociation reactions. The reported (total) redissociation rates at 298 K are both about a hundred times higher than the values obtained in this work by the more reliable approach of combining experimental O_2-addition rates with statistical-thermodynamics calculated equilibrium constants. Those much higher reported results[68] are largely due to the adopted dissociation energies for both peroxy isomers being 2.2 kcal mol^{-1} lower than our present high-level results (and even around 1 kcal mol^{-1} below our earlier low-level results). Of course, at our 100 times lower k_{-O2} rates, the steady-state internal energy distributions of these peroxys should deviate much less — and hence only negligibly — from the thermal distributions than estimated in that recent paper.

Isomerisations of the Z-δ-OH-peroxys by 1,6-H shift and of the β-OH-peroxys by 1,5-H shift

The rate coefficients k(*Z*-δ 1,6-H) of the 1,6-H shift in the *Z*-δ-OH-peroxys and k(β 1,5-H) of the 1,5-H shift in the β-OH-peroxys, are evaluated using multi-conformer transition state theory, MC-TST,[45] e.g. for the 1,6-H shifts:

$$k(Z\text{-}\delta\ \ 1,6\text{-H})(T) = \kappa(T)\frac{k_B T}{h}\frac{\sum Q^{\ddagger}_{TS}}{\sum Q_{Z\text{-}\delta\text{-OH-peroxy}}} \times e^{-\frac{E_0}{k_B T}} \qquad (2)$$

in which h is Planck's constant and k_B Boltzmann's constant; $\sum Q^{\ddagger}_{TS\ 1,6\text{-H}}$ and $\sum Q_{Z\text{-}\delta\text{-OH-peroxy}}$ are the multi-conformer partition functions of the TS for the 1,6-H shift and of the *Z*-δ-OH-peroxy considered, respectively, evaluated as above, with each individual Q_i weighted by the relative thermal population $\exp(-\varepsilon_i/k_B T)$; E_0(1,6-H) is the

energy barrier or difference between the energies of the lowest conformers of TS and peroxy radical, respectively, both computed at the high CC//QC level of theory; $\kappa(T)$ is the average tunneling factor, obtained by weighting the individual κ_i by the individual partition functions Q_i of the TS conformers, i.e.: $\kappa = \Sigma(\kappa_i \times Q^{\neq}_i)/\Sigma Q^{\neq}_i$. For Case I only two TS conformers and For Case II three TS conformers were taken into account, the contribution of all higher conformers being minor.

The crucial barrier height values for the 1,6-H shifts thus found are E_0(1,6-H) = 19.62 and 18.11 kcal mol^{-1} for Cases I and II, respectively. The about 1.5 kcal/mol lower barrier for Case II, found systematically at all levels of theory, is due to the stabilizing effect of the methyl-group on that carbon in the allylic product. A schematic PES for the 1,6-H shift, Case I, through the lowest TS conformer, is depicted in Figure 3. Worth noting, the CC//QC barriers above are supported by the 19.46 and 17.95 kcal mol^{-1} values computed at M06-2X level, but they are significantly higher than the lower-level CBS-APNO results of our earlier communication.[20] However, the higher barriers are compensated by the M06-2X-based multi-conformer partition functions of the *Z*-OH-peroxy reactants being substantially lower than the earlier, lower-level B3LYP-based data,[20] as already implied above. Another important difference are the tunneling factors, which were earlier evaluated in a unidimensional zero-curvature (ZCT) WKB-approximation. As recently pointed out by Zhang and Dibble,[46] ZCT underestimates tunneling in 1,4-H and 1,5-H shifts in C_5-peroxy radicals by factors 3 to 4 compared to the much more reliable small-curvature SCT results, which, on the other hand, these authors found to be fairly well reproduced by the asymmetric Eckart barrier approximation. Therefore, we presently adopt the Eckart approximation, using the code

from Coote et al.[69] The scaled[70] imaginary frequencies of the two lowest conformers of TS(*Z*-δ 1,6-H)(I) for example, computed at M06-2X using an ultra-fine grid,[71] are 1735.45 and 1820.53 cm^{-1}, while the reverse barriers were taken equal to the forward barriers in order to account for the allyl-resonance-induced widening of the barrier starting at ≈15 kcal mol^{-1} below the top, as discussed below and illustrated in Figure 3. The resulting tunneling factors $\kappa_i(298\ \mathrm{K})$ of 102 and 161 are indeed around 4 times higher than the earlier ZCT values of about 28.[20] Details on the strongly *T*-dependent tunneling factors κ_i of the contributing TS conformers for both Cases are given in Table S4. It should be stressed here that the 1,6-H shifts, which are at the heart of the new chemistry in LIM, occur for over 99% by hydrogen atom tunneling. Finally, the fall-off factors at 1 atm, calculated using the standard RRKM approach, are found to be ≥ 0.99 at all relevant temperatures, and were therefore taken equal to 1.

The rate coefficient values computed at 280, 285, 298, 315 and 320 K, listed also in Table S3, can be fitted within 0.25% by the equations

$$k(Z\text{-}\delta\ 1,6\text{-H})(\mathrm{I})(T) = 3.56 \times 10^{10} \times \exp(-8591/T) \times \exp(1.027\times10^{8}/T^{3})\ s^{-1} \quad (3a)$$

$$k(Z\text{-}\delta\ 1,6\text{-H})(\mathrm{II})(T) = 1.07 \times 10^{11} \times \exp(-8174/T) \times \exp(1.000\times10^{8}/T^{3})\ s^{-1} \quad (3b)$$

in which the second exponential functions featuring T^{-3} in the argument, express mainly the strongly curved negative *T*-dependence of the tunneling factors.

The rate coefficient values at 298 K are $k(Z\text{-}\delta\ 1,6\text{-H})(\mathrm{I})(298) = 0.520\ s^{-1}$ and $k(Z\text{-}\delta$ 1,6-H)(II)(298) = 5.72 s^{-1}, respectively. These values are not too different from our earlier, low-level results,[20] but, as explained above, the accord is rather fortuitous.

In the same very recent paper mentioned above, a $k(Z\text{-}\delta\ 1,6\text{-H})(\mathrm{I})$ value at 298 K of 6.5 s^{-1} was reported,[68] i.e. 12.5 times our present value, the reason for that higher value

being that the authors adopted our low-level original estimate of the barrier height,[20] *ca.* 1.7 kcal mol^{-1} lower than our present higher-level result. On the other hand, Taraborrelli et al.[14] reported theoretical rate coefficients $k(Z\text{-}\delta$ 1,6-H) that are 2.5 to 3 times lower than our present results, computing (relative) single-point energy barriers at the high CCSD(T)/aug-cc-pVTZ level but on B3LYP-optimized geometries and using B3LYP-based partition functions as in our earlier papers.[20] The lower rates are explained mainly by the neglect of London dispersion in B3LYP causing the relative energy of the lowest, H-bonded TS to be too high by about 1.3 kcal/mol compared to M06-2X, such that its contribution to the total 1,6-H shift rate would be minor; in our computations, which account properly for the crucial London dispersion effects, the H-bonded TS contributes as much again as the other TS conformers combined to the total 1,6-H shift rate.

At this stage, first of all, it is necessary to most strongly emphasise that the $k(Z\text{-}\delta$ 1,6-H) values, of order 1 s^{-1} at ambient temperatures, are the *isomer-specific* rate constants for the elementary reactions of the *Z*-δ-OH peroxys, and, contrary to what was erroneously stated or implied in two recent reviews,[54,72] not the formal "bulk rate coefficient" for isomerisation of *the pool* of isoprene-peroxys, as was measured by Crounse et al.[27] In fact, these two very distinct quantities differ by orders of magnitude, as shown in the next section.

An important difference compared to our earlier, lower-level results is that at our present levels of theory, which account properly for London dispersion, the lowest of the two contributing TS conformers for the 1,6-H shift of Case I conserves the H-bond throughout the reaction, leading directly to the most stable, H-bonded *Z,Z′*-conformer of the allylic product radical, as shown in Figure 3. Similarly for Case II, one of the lowest

TS conformers conserves the H-bond (see Table S2). The other contributing TS conformer(s) for Cases I and II are connected to open, i.e. non-H-bonded product radicals, with the OH group pointing outwards. However, these nascent products are formed with an internal energy of some 21 kcal mol^{-1} (including 4 kcal mol^{-1} thermal energy but accounting for the tunneling occurring on average about 3 kcal mol^{-1} below the barrier top). Of this total, about 14 kcal mol^{-1} is owed to allyl-resonance stabilization, which however can become active only after the H atom has quasi-completely migrated such that a half-occupied p orbital (together with three sp^2 bonding orbitals) develops on carbon 1, which can then align and overlap with the two existing p orbitals of the $>C_2=C_3<$ double bond. The associated potential energy decrease appears as vibration energy of the allyl mode, i.e. simultaneous asymmetric stretching of the bent C_1-C_2-C_3 frame and counter-rotation about the two C-C axes. The so dynamically induced internal rotation of the $HOC_1^{\bullet}H$ moiety about C_1-C_2 should allow the hot product radical to overcome the 12 to 13 kcal mol^{-1} barrier leading to the 5 kcal mol^{-1} more stable H-bonded *Z,Z'*- product isomer displayed in Figure 3 for Case I. As discussed in detail in a next section, this is relevant for the subsequent fates of the allylic product radicals of the 1,6-H shifts. It is useful to already add here that because of the allyl character, the product radicals feature two radical sites and hence one expects subsequent formation of two different peroxy radicals, in similar quantities.

Our best-level CC//QC results for the barriers of the concerted 1,5-H shifts in the β-OH-peroxys are 21.29 for Case I and 21.03 kcal mol^{-1} for Case II, with the M06-2X results of 21.68 and 21.42, respectively, even somewhat higher. These data are significantly higher that our earlier, lower-level CBS-APNO and B3LYP values. In the

partition function ratios, 3 (Case I) and 2 (Case II) contributing TS conformers and *ca.* 25 conformers of the β-OH-peroxys are accounted for. The tunneling factor, in the asymmetric-Eckart approximation (see Table S4 for details) is small, only around 3 at 298 K, because of the low imaginary frequencies and the rapid widening of the barrier from *ca.* 4 kcal mol^{-1} below the top down, both due to the concerted nature of the reaction that results in OH + CH_2O + MVK for Case I and in OH + CH_2O + MACR for Case II, without stable intermediate.[20] The isomer-specific rate coefficients for the 1,5-H shifts of the β-OH-peroxys computed for the 280 - 320 K range, listed in Table S3, can be represented within 0.25% by the expressions

$$k(\beta\ 1,5\text{-H})(\text{I})(T) = 1.04 \times 10^{11} \times \exp(-9746/T)\ s^{-1} \quad (4a)$$

$$k(\beta\ 1,5\text{-H})(\text{II})(T) = 1.88 \times 10^{11} \times \exp(-9752/T)\ s^{-1} \quad (4b)$$

with values at 298 K of 6.5×10^{-4} s^{-1} for Case I and 1.15×10^{-3} s^{-1} for Case II. These rate coefficients are substantially lower than our preliminary earlier results,[20] and much lower than the even 5 times higher values we tentatively adopted later[21] to explain the additional MVK and MACR observed by Paulot[4] by the 1,5-H isomerisation reactions. The present results are about 1.5 to 2 times higher than the theoretical predictions of da Silva et al.[23] based on computed energy barriers taken as the average of two composite methods (G3SX and CBS-QB3), although with a reported possible error of 2 kcal mol^{-1}, amounting to an error factor of 25 on the rates.

The present rate coefficient results, based on the CC//QC barriers, are some 20 times smaller than the combined rates of the traditional peroxy reactions in relevant conditions, meaning that the 1,5-H shifts of the β-OH-peroxys are quasi-negligble — except at the highest relevant temperatures — in agreement with the experimental findings of Crounse

et al.[27] Our average k(1,5-H) result of about 2×10^{-3} s^{-1} at 305 K suggests that the 1,5-H shifts of the β-OH-peroxys could have contributed only in a minor way to the about 60% OH regeneration observed in the recent chamber study of Fuchs et al.[18] at this temperature, given the peroxy removal rate around 0.035 s-1 by the traditional reactions in their conditions.

Steady-state population fractions of the Z-δ-OH-peroxys and bulk peroxy isomerisation rate through the 1,6-H shifts

The empirical bulk peroxy isomerisation "coefficient", as introduced by Crounse et al. who denoted it as k_{isom},[27] but designated in this work as k(bulk 1,6-H), is defined as the volumic rate of the 1,6-H shifts of the *Z*-δ-OH-peroxys divided by the total concentration of all hydroxy-isoprenyl peroxys. It is readily seen that k(bulk 1,6-H) is simply equal to the isomer-specific rate coefficient k(*Z*-δ 1,6-H) multiplied by the actual steady-state fraction f(*Z*-δ) of the *Z*-δ-OH-peroxys, or rather the sum for the two Cases weighted by their branching fraction (Br = 0.62 for Case I and 0.31 for Case II):

$$k(\text{bulk 1,6-H}) = \text{Br(I)} \times f(Z\text{-}\delta)(\text{I}) \times k(Z\text{-}\delta \ \text{1,6-H})(\text{I}) + \text{Br(II)} \times f(Z\text{-}\delta)(\text{II}) \times k(Z\text{-}\delta \ \text{1,6-H})(\text{II}) \quad (5)$$

Now that the rates of all reactions affecting the populations of the β-, *Z*-δ- and *E*-δ-OH-peroxy isomers are derived, their steady-state fractions f(β)(I), f(*Z*-δ)(I), f(*E*-δ)(I) and f(β)(II), f(*Z*-δ)(II), f(*E*-δ)(II) can be derived for any given condition of temperature and traditional peroxy removal rate, k_{tr}, and hence k(bulk 1,6-H) can be evaluated. All rate coefficient expressions for Cases I and II are grouped in Table S5.

As detailed in section S4 (Supporting Information), the condition for full equilibrations such as β-OH-peroxy $\rightleftharpoons$ *Z*-δ-OH-peroxy (Ra) in our complex system is

essentially that the redissociation rates of each of the two peroxy isomers involved are much higher than their removal rates by all the other reactions together.

The actual rate coefficients, which can be found from Table S5, and with k(298 K) values displayed in Figures 1 and 2, show that the above condition is not generally met for the relevant temperatures of *ca*. 280 - 305 K and k_{tr} range 0.01 - 0.1 s^{-1}, i.e. for low and moderate NO levels. (Only the less important analogous equilibrium (Rb) for Case I is always established within a few percent). In section S4, the departures from equilibrium are discussed in some detail, and reduced analytical expressions for the real, steady-state peroxy population fractions are derived that give the fractions f(*Z*-δ) and hence also the bulk rates k(bulk 1,6-H) with a precision better than ±2% over the relevant T and k_{tr} ranges above. Also, the rigorous population fractions as well as bulk rates k(bulk 1,6-H) (the latter shown in Figure S3) and the yields of the various 1st-generation products (see Figure 4) as functions of k_{tr} and of T have been obtained by box-modelling on the full, explicit mechanism.

For Case I, the steady-state [*Z*-δ]/[β] ratio and f(*Z*-δ) fraction in the relevant k_{tr} range are considerably higher than the equilibrium values and increase substantially as k_{tr} becomes higher, in particular at the lower temperatures; the departures from equilibrium remain below 5% throughout this k_{tr} range only for $T \geq 310$ K. The reason for this behavior is that firstly at lower temperatures the *Z*-δ-OH- and β-OH-peroxys redissociate (far) too slowly to ensure equilibration such that the [*Z*-δ]/[β] ratio is determined to a larger extent by their (near-unity) initial formation ratio (see Figure 1) and their respective rates of irreversible removal; secondly, at higher k_{tr} the absolute concentrations of the β-OH-peroxys and *E*-δ-OH-peroxy that are removed almost solely by the

traditional reactions will decrease substantially, whereas [*Z*-δ-OH-peroxy] will be much less affected since k(*Z*-δ 1,6-H) is much larger than k_{tr} in the considered range. For Case II, the high k(*Z*-δ 1,6-H)(II) values of order 1 - 10 s^{-1} preclude the establishment of the equilibrium at any relevant T and k_{tr}, such that the [*Z*-δ]/[β] ratio is mostly only 0.1 - 0.5 times the $\{[Z\text{-}\delta]/[\beta]\}_{eq}$ value, but showing a strong increase with k_{tr} for the same reason as in Case I. As an example, at T = 298 K and k_{tr} = 0.025 s^{-1}, one has f(*Z*-δ)(I) = 1.35 × 10^{-2} and f(*Z*-δ)(II) = 2.72 × 10^{-3}, showing that the fraction of *Z*-δ-OH-peroxys is very low, in particular for Case II, such that — and this needs strong emphasis — the k(bulk 1,6H) are two to three orders of magnitude smaller than the isomer-specific rate coefficients k(*Z*-δ 1,6-H).

It should be remarked that the calculated steady-state f(*Z*-δ) and therefore also the k(bulk 1,6H) can depend indirectly on the choice of the k_{+O2}^{bulk} (see above), because the k_{-O2} as derived above are all directly and simultaneously proportional to k_{+O2}^{bulk}, and higher k_{-O2} values should bring the [*Z*-δ]/[β] ratios closer to equilibrium. However, as shown in Figure S4, the product distribution for Case I over the k_{tr} range of 0.01 - 0.1 s^{-1} is quite robust against such a simultaneous change of all k_{-O2} (through the choice of k_{+O2}^{bulk}), while the product yields for Case II are somewhat affected by it.

It is of interest to note that the steady-state f(*Z*-δ) fractions for Case I are about 3 to 6 times lower, and those for Case II more than an order of magnitude lower than found earlier at lower levels of theory,[20] mainly because of the presently computed lower partition function ratio of the *Z*-δ-OH- and β-OH-peroxy isomers and slower redissociations of both isomers, due to a large extent to the London dispersion effect on the H-bond strengths now being properly accounted for. Mainly for that reason, the

present *k*(bulk 1,6-H) values too are about an order of magnitude lower than the original rough estimates.

Of major importance is that, based on the set of present rate coefficients (see Table S5), both the *f*(*Z*-δ) and therefore the bulk isomerisation rate *k*(bulk 1,6-H) (see Figure S3) show a manifest increase with k_{tr}, or, in other words: "*k*"(bulk 1,6-H) is not a true rate *constant*, but increases nearly linearly with the isoprene-peroxy sink rate by the traditional reactions k_{tr} (see section S4):

$$k(\text{bulk 1,6-H})(\text{I}) = 9.50 \times 10^{7}\ \text{s}^{-1} \times \exp(-7009/T) + 1.79 \times 10^{-7} \times \exp(+3722.5/T) \times k_{tr} \quad (5a)$$

$$k(\text{bulk 1,6-H})(\text{II}) = 3.80 \times 10^{13} \times \exp(-10745/T)\ \text{s}^{-1} + 5.82 \times 10^{-2} \times \exp(+476.3/T) \times k_{tr} \quad (5b)$$

with *k*(bulk 1,6-H)(total) = 0.62 × *k*(bulk 1,6-H)(I) + 0.31 *k*(bulk 1,6-H)(II). (see equation 5, above). For example, at 295 K, the bulk rate increases from 0.006 to 0.017 s^{-1} between k_{tr} = 0.01 s^{-1} and k_{tr} = 0.1 s^{-1}. The nearly-perfect linear increase with k_{tr} over the relevant *T* and k_{tr} ranges can be exploited for the implementation of the 1,6 H-shift reactions in large-scale models, by splitting the isomerisation into a constant-rate unimolecular component and pseudo-bimolecular reactions with HO_2, NO and RO_2 accounting for the dependence of the bulk rate on k_{tr}.

The overall uncertainty on the derived *k*(bulk 1,6-H) is estimated based on the probable errors on the six parameters affecting *k*(*Z*-δ 1,6-H) and *f*(*Z*-δ). The first two are the barrier height of the 1,6-H shift and the Δ*E* between the *Z*-δ-OH- and β-OH-peroxys; as objective estimates available for the expected errors on the Δ*E*, we adopted the

differences, of 0.16 and 0.19 kcal mol^{-1}, respectively, between the values computed at the independent high-quality CC//QC and M06-2X levels used in this work. Further, we assumed a factor 1.5 error on the tunneling factor; a factor of 1.3 each for the MC-partition function ratios for the 1,6-H shift and the $\{[Z\text{-}\delta]/[\beta]\}_{eq}$ equilibrium constant; and a factor 1.3 error on the calculated departures from that equilibrium. Error propagation thus yields an overall uncertainty estimate on k(bulk 1,6-H) of a factor ≈ 2, or +100%/-50%. The estimated uncertainty of a factor ~2 on the bulk rate coefficient is considerably smaller than the reported uncertainty of a factor 5 to 10 on just the isomer-specific 1,6-H shift rates of the *Z*-δ-OH-peroxys in our earlier work.[20]

Peroxy isomerisation Yields. Comparison with experimental results

As seen on Figure 4, the LIM1-predicted 1,6 H-shift yield is found to range between 15% and 50% in typical non-urban atmospheric conditions, whereas the 1,5 H-shift yield is very low. A reduced version of LIM1 has been implemented in the global chemistry model IMAGES.[24] The isoprene oxidation mechanism at high-NOx is based on the MIM2 mechanism[73] with updates described in Stavrakou et al.[24,74] The traditional reaction products of the δ-hydroxy-peroxy radicals from isoprene are omitted, since their yields are negligible in relevant atmospheric conditions. The 1,6 isomerisation reactions are accounted for through bulk reactions of the isoprene peroxys with rates which are linearly dependent on their traditional sink rate (k_{tr}), as described above. The formation of di-hydroperoxy carbonyl peroxy radicals (see below) is not considered here, since their subsequent chemistry remains to be elucidated. For a similar reason, the further photochemistry of HPALD is highly simplified, as in Stavrakou et al.[24] Whereas this

simplified representation is sufficient for the purpose of estimating the isomerisation yields, it is not expected to provide an accurate assessment of HOx regeneration in isoprene oxidation, given the importance of secondary chemistry. The global and annually averaged yields of the 1,6 and 1,5 H-shifts are estimated to be 28% and 2.3%, respectively. The distributions of the yields are displayed in Fig. S5 and S6. The uncertainty on k(bulk 1,6-H), above, translates into a relative error on the global 1,6-H yield of +54%/-40%, which brackets this yield between 17 and 43%.

We evaluate the theoretical yields using an explicit chemical model against the measured formation rates of HPALD and other stable products in the low-NOx isoprene oxidation experiments of Crounse et al.[27] at Caltech. As discussed in the next section, HPALD formation is only one of the two major possible pathways following the 1,6 H-shift, with an estimated branching fraction of 50%. The radical source in the experiments was provided by CH_3ONO photolysis using black lights irradiating above 300 nm. The photolysis rates are calculated from the lamp spectrum[75] and the reported photolysis rate of NO_2 (2.8×10^{-5} s^{-1})[27]. The product $J(CH_3ONO) \times [CH_3ONO]$ is estimated from the balance between HOx production and HOx removal which is obtained, to a good approximation, from the reported production rates of hydroperoxides and nitrates, i.e. $2 \times (P(H_2O_2) + P(ISOPOOH)) + P(ISOPNO_2)$.

As seen on Table 1, a reasonable agreement is found between the measured and simulated product formation rates at three different temperatures. LIM1 appears to overestimate the measured HPALD formation rate by a factor which is almost constant (~1.8) for all experiments. This discrepancy is compatible with the combined experimental and theoretical uncertainties. The observed steep increase in HPALD

between 295 and 318 K (factor of 4), well reproduced by LIM1, is primarily due to the temperature dependence of the peroxy dissociation rates: indeed, model results obtained when ignoring peroxy dissociation reactions show very little dependence of HPALD formation on temperature (Table 1), in spite of the strong temperature dependence of the isomerisation rates of *Z*-δ-OH-peroxys. Since isomerisation is by far the dominant sink reaction of those *Z*-δ-OH-peroxys at the low-NO conditions of the experiments (as of most atmospheric conditions), the main limiting factor to HPALD formation is the formation rate of the *Z*-δ-OH-peroxys. This rate is constant when neglecting peroxy dissociation, but it increases with temperature in LIM1 due to the conversion of β-OH- to *Z*-δ-OH-peroxys. In conclusion, the Caltech measurements appear to validate not only the formation of HPALD, but even more — and quasi-quantitatively — the reality and importance of the O_2-elimination reactions of the hydroxyperoxys resulting in their rapid interconversion under low-NO conditions.

Bulk peroxy 1,6-D isomerisation rate in the OH-initiated oxidation of per-deuterated isoprene and comparison with experiment

Following a suggestion by a reviewer, we have also computed the bulk peroxy 1,6-D isomerisation rate, in order to compare the theoretically predicted kinetic isotope effect with the experimental *k*(bulk *Z*-δ) H/D ratio of 15.0 at T = 298 K for normal/per-deuterated isoprene from Crounse et al., in conditions of $k_{tr} \approx 0.021$ s^{-1}. [27] In fact, this experimental result is unexpectedly low and needs to be rationalized: the usual primary kinetic isotope effect for H/D "abstraction" of a factor ≈5 at 298 K due to the adiabatic

barrier difference of ≈1 kcal mol^{-1} is accompanied here by an expected κ^H/κ^D tunneling factor ratio of about $(\kappa^H)^{0.5} \approx 8$ - 12.

The D atoms of isoprene-D_8 are not involved in any chemical or hydrogen bonding that could affect in any significant way the reaction rates and equilibria governing the peroxy isomer interconversions and therefore all these parameters were considered identical to the isoprene-H_8 case. To quantify the important primary and secondary kinetic isotope effects above, the differences in 1,6-D/H shift adiabatic barrier heights between the D- and H-cases and the ratios of the pertaining Q(TS)/Q(reactant) partition function quotients were computed at the M06-2X level for all contributing TS conformers for both Cases I and II. The results are tabulated in Table S6, together with the D-tunneling factors at 298 K obtained in a similar way as for the H-cases. The energy barriers for the D-shifts are indeed about 0.8 to 1.2 kcal mol^{-1} higher, due to the zero-point vibration energy difference, while the D-tunneling factors are 8 to 14 times lower than for H. Including also the minor changes (± 5 to 20 %) in the Q(TS)/Q(reactant) quotients, the two kinetic isotope effects together result in k(*Z*-δ 1,6-D) values lower than the k(*Z*-δ 1,6-H) by a factor 45.0 for the *Z*-δ-OH-peroxys of Case I and 65.8 for Case II, or in terms of the absolute values: k(*Z*-δ 1,6-D)(I) = 0.0115 s^{-1} versus k(*Z*-δ 1,6-H)(I) = 0.520 s^{-1}, and k(*Z*-δ 1,6-D)(II) = 0.087 s^{-1} versus k(*Z*-δ 1,6-H)(II) = 5.72 s^{-1}, all at 298 K. However, and this should again be strongly emphasized, Crounse et al. measured not the H/D ratio of the isomer-specific k(*Z*-δ 1,6-H/D), but the ratio of the bulk peroxy isomerisation rates: k(bulk 1,6-H) / k(bulk 1,6-D) = [f_H(*Z*-δ) × k(*Z*-δ 1,6-H)] / [f_D(*Z*-δ) × k(*Z*-δ 1,6-D)]. For the Case II peroxys, the ratio of the steady state fractions f_H(*Z*-δ)/f_D(*Z*-δ) ratio is expected to be << 1, because the very fast 1,6-H shift (see Table S5) keeps the

Case II $f_H(Z\text{-}\delta)$ far below equilibrium (see above) while the much slower 1,6-D shift should allow much higher $f_D(Z\text{-}\delta)$, close to their equilibrium value. Obviously, The precise $f_H(Z\text{-}\delta)/f_D(Z\text{-}\delta)$ ratio will be controlled too by the rates of the (indirect) β-OH-peroxy $\rightleftharpoons$ *Z*-δ-OH-peroxy interconversions. Using equations (SB1') and (SB2) in Section S4 (Supporting Information) the $f_D(Z\text{-}\delta)$ *versus* $f_H(Z\text{-}\delta)$ for T = 298 K and k_{tr} = 0.021 $s^{-1}$are found to be 0.0151 *versus* 0.0130 for Case I and 0.0201 *versus* 0.0025 for Case II, the latter meaning an $f_H(Z\text{-}\delta)/f_D(Z\text{-}\delta)$ ratio as low as 0.125. It follows that, always at 298 K and for k_{tr} = 0.021 s^{-1}, *k*(bulk 1,6-D)(I) = 1.75 × 10^{-4} s^{-1}, or a factor 39 lower than *k*(bulk 1,6-H)(I), but on the other hand *k*(bulk 1,6-D)(II) = 1.75 × 10^{-3} s^{-1} or only a factor 8.2 lower than *k*(bulk 1,6-H)(II). Thus, accounting for the respective branchings of 0.62 and 0.31 for Cases I and II, the overall *k*(bulk 1,6-D) = 6.51 × 10^{-4} s^{-1} for isoprene-D_8, *versus* *k*(bulk 1,6-H) = 8.67 × 10^{-3} s^{-1} for isoprene-H_8, i.e. a theoretical *k*(bulk) H/D ratio of 13.3. That this result is in good agreement with the experimental *k*(bulk) H/D ratio of 15.0 at 298 K from of the expressions of Crounse et al. for $k_{tr} \approx 0.021$ s^{-1},[27] strongly supports our predicted peroxy-isomer interconversion rates. Interestingly, this analysis predicts also that for isoprene-D_8 the (slower) peroxy isomerisation is mainly due to the Case II peroxys, whereas for normal isoprene Cases I and II contribute roughly equally. Also, the above analysis demonstrates once again the crucial distinction that must be made between the isomer-specific rate coefficients and the experimentally accessible bulk-peroxy rate coefficients — a distinction that unfortunately has been overlooked even in review papers.

Two major pathways following isoprene-peroxy isomerisation by 1,6-H shift: to *Z*-HPALDs and to di-HPCARP radicals

The allylic product radicals of the 1,6-H shifts, expected to be formed predominantly as the more stable, H-bonded, cyclic *Z,Z'*- conformers (see Figure 3) should arise with a nascent internal energy of around 25 kcal mol^{-1} (see above). In principle, some chemically activated reactions might therefore occur promptly. We have thoroughly examined some 10 possible unimolecular reactions, but found the barriers for all of them to be too high to be of major importance — except for the internal rotation of the initially "open" product conformers to yield the more stable H-bonded ones discussed above. The most likely decomposition reactions, of which the transition states are shown in Figure S7 for Case I, are (i) elimination of H_2O to form an oxy radical O=CH-C(CH_3)=CH-$CH_2O^{\bullet}$; (ii) concerted elimination of OH to yield a hydroxy-methyl-butenal O=CH-C(CH_3)=CH-CH_2OH; (iii) concerted expulsion of an OH to form an epoxide; and (iv) the elimination of H_2O_2 giving an O=CH-C(CH_3)=CH-$C^{\bullet}H_2$ allylic radical. However, at the sufficiently high and reliable levels of theory M06-2X and/or CC//QC, the barriers for the three first, most favorable reactions are found to be around 17 kcal mol^{-1} or higher; which for the given nascent energy content is too high for these reactions to outrun collisional stabilisation. The reason why the barriers to (i) H_2O elimination and (iii) OH elimination here are substantially higher than reported for the similar reactions of hydroperoxyalkyl radicals,[76] is that for our case the ≈ 14 kcal mol^{-1} allyl-resonance stabilization of the reactant is lost in the product. It is estimated therefore that the various prompt reactions examined contribute no more than some 10% together, and possibly much less.

After collisional stabilisation, the allylic product radicals should add O_2 to form two different allylperoxys, the "1st peroxy" and "2nd peroxy", as depicted in Figures 1 and 2, and in the detailed subsequent PES for Case I in Figure 5 (the mechanisms and the PES for Case II being analogous). O_2 addition should show a slight preference for allylic carbon 2 with its higher spin density of 0.58 *vs* 0.42 for carbon 1. It has been ascertained that both additions can occur without any significant barrier, owing (again) to the simultaneous formation of H-bonds. The "1st peroxy" rapidly yields a strongly H-bonded complex of HO_2 and a carbonyl over a barrier of 12.5 kcal mol^{-1}, followed by decomposition of the complex into free HO_2 and *Z*-1-hydroperoxy-2/3-methyl-but-2-enal (*Z*-HPALD), requiring 12.0 kcal mol^{-1}. The first step, through a very rigid TS, is rate controlling and may occur promptly given the ≈ 25 kcal mol^{-1} nascent internal energy of "1st peroxy". In any case, its overall decomposition into HO_2 + *Z*-HPALD will be much faster than the potential re-dissociation of this allylperoxy radical.

The "2nd peroxy", somewhat less stable than the first, undergoes a fast enolic 1,6-H shift over an unusually low barrier of only 8.6 kcal mol^{-1} similar to the shift we discovered for the 1st-generation production of hydroxy-acetone and glycolaldehyde in isoprene oxidation at high NO.[77] Here too, the reaction will be prompt, and outrun the re-dissociation of the "2nd peroxy" by orders of magnitude. However, we do not exclude that some 10 or 20% of the products of the 1,6-H shifts arise as "open" *Z,E'*-conformers with the OH pointing outwards; these cannot undergo the enolic 1,6-H shift and their sole fate should be redissociation and hence finally conversion to the "1st peroxy" isomers that can still rapidly yield HPALDs plus HO_2. This is why we adopt here effective branchings to the two peroxys of 0.5 : 0.5, despite the somewhat higher spin density on allylic carbon 2.

The doubly-H-bonded, vinoxy-stabilized product radical from the 1,6-H shift of the "2nd peroxy", with nascent internal energy of about 28 kcal mol^{-1}, might undergo several possible prompt unimolecular reactions, including concerted OH expulsion and epoxide formation, but all have been found to face too high barriers (≥ 18 kcal mol^{-1}, partly on account of the lost vinoxy resonance in the TS's) to compete with collisional stabilisation. Therefore, it should instead rapidly add another O_2 — a third already — to form a di-hydroperoxy-carbonyl-peroxy radical (di-HPCARP), which keeps the double H-bond, and should arise with a nascent internal energy of some 20 - 25 kcal mol^{-1}, which is insufficient for important prompt reactions, such that the di-HPCARP should collisionally thermalize before reacting.

Fate of HPALDs: fast photolysis regenerating OH, and OH-neutral reaction with OH

In the earlier proof-of-concept papers on LIM,[20,21] we proposed fast photolysis of the *Z*-4-hydroperoxy-2/3-methyl-but-2-enals (HPALDs) into OH and oxy radicals (O=CH-$C(CH_3)$=CH-$CH_2O^\bullet$ in Case I and O=CH-CH=$C(CH_3)$-$CH_2O^\bullet$ in Case II), assuming similar absorption cross sections as for the analogous α,β-enones MVK and MACR, but — very different from the latter — with near-unit quantum yield (QY), and hence J-values of order 5×10^{-4} s^{-1}. The high-QY mechanism proposed was an avoided crossing of the excited S_1 state of the O=C-C=C enone chromophore (or its triplet counterpart T_1) with the repulsive excited S_2 state of the -OOH hydroperoxide chromophore (or its triplet counterpart T_2). The fast photolysis of HPALDs into OH with near-unit QY has since

then been confirmed experimentally by Wolfe et al. for a HPALD proxy, *E*-4-hydroxyperoxy-hex-2-enal.[28]

A detailed theoretical investigation is in progress on the intricate photo-physical and molecular mechanism of the *Z*-HPALD photolysis process and the subsequent chemistry. This ongoing work will be reported elsewhere when finalized. A detailed discussion of the findings so far is beyond the scope of this article, but some conclusions having direct bearing on the potential of the co-product oxy radical, above, to re-generate additional hydroxyl radicals should be outlined here. First, though we have theoretically located a transition state for an avoided crossing as proposed, we have now identified an unexpected but much faster mechanism to OH + oxy radical, while still another mechanism could also become competitive in particular at higher excitation energies; these two dominant pathways have still to be kinetically quantified. Secondly, of prime importance, the dynamics of both these faster mechanisms are such that the oxy radical, co-product of OH, will be formed with a very high internal energy of some 35 - 40 kcal mol^{-1}, much higher than expected for the originally assumed photolysis mechanism, such that the chemical fate of these oxy co-products will be quite different from that originally proposed.[20,21] Thirdly, the oxy radicals can be formed either as the *E*- or the ca 3 kcal mol^{-1} less stable *Z*-conformers, which we found can readily interconvert *via* an unusual mechanism through a nearly-iso-energetic oxyranyl intermediate, over CC//QC-computed energy barriers of only 5 to 8 kcal mol^{-1}:

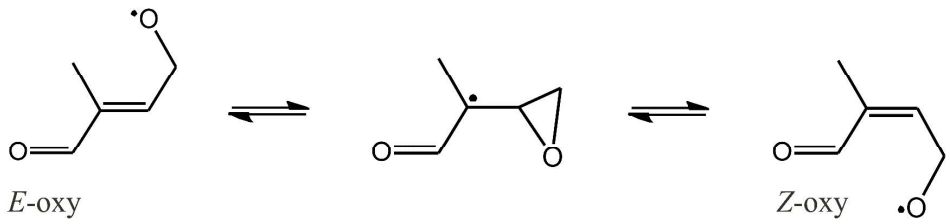

As a result, two prompt, chemically activated pathways are open for these oxy radicals, shown below for Case I: a nearly barrierless 1,5-H shift of the aldehyde hydrogen in the *Z*-oxy, exothermal for 17 kcal mol^{-1}, possible for both Cases I and II; and a 1,5-H shift of a methyl-hydrogen in the *E*-oxy of Case I facing a CC//QC-computed barrier of 8.86 kcal mol^{-1} and exothermal for 19 kcal mol^{-1}:

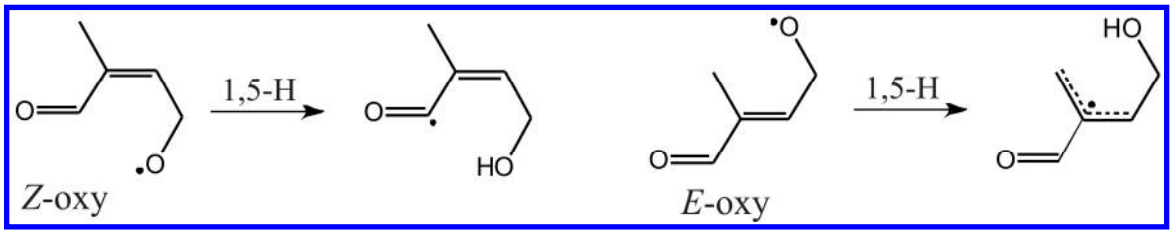

The expected subsequent chemistry, that still needs to be fully characterized and kinetically quantified and hence to be reported separately, is schematised in Figure S8 for the *Z*-oxy. The relative energies and barrier heights mentioned below, are all computed at the M06-2X level. The nascent acyl radical from the prompt aldehyde-H shift in the *Z*-oxy contains already over 50 kcal mol internal energy, enough to promptly overcome the 23 kcal mol^{-1} barrier for CO loss and so form a vinyl-type radical, which can rapidly interconvert from a *Z*- to an *E*-conformer over a low barrier of $\leq$ 5 kcal mol^{-1} (Case I) resulting in their thermal equilibration with *Z*- / *E*- ratio governed mainly by the relative stabilities. Fast O_2 addition should then give rise to two chemically activated vinylperoxy conformers with nascent internal energies of about 45 kcal mol^{-1}, but with very different subsequent fates. A fast and dominant 1,5-H shift over a barrier of only 16.5 kcal mol^{-1} is open to the *Z*-vinylperoxy conformer, whereas the *E*-counterpart can only undergo "traditional" reactions with NO, HO_2, RO_2 or NO_2. The H-shift in the *Z*-vinylperoxy forms an unstable 1-hydroperoxy-1-methyl-3-OH-allyl radical that spontaneously expels OH,[78] to form a strongly H-bond-stabilized ketone-enol — which can be termed hydroxy-

vinylmethylketone — and is the more stable tautomer of the β-diketone formylacetone, similar to the homologous ketone-enol tautomer of acetylacetone.[79] Again by analogy with acetylacetone, it should photolyze quickly into OH and a (strongly resonance-stabilized) radical[80] at a rate that can be estimated at about (2 - 3) × 10^{-4} s^{-1} for an overhead sun using the known absorption cross sections for the (allowed !) π,π* transition of acetylacetone[81] and assuming a quantum yield of unity. However, similar to acetylacetone,[82] this ketone-enol is expected to react also very quickly with OH, with a rate coefficient close to 1 × 10^{-10} cm^3 s^{-1}. The net OH budget of the *Z*-oxy chemistry is therefore uncertain, and may be decided by the subequent chemistry of the (unknown) photo-product radical and of the OH-adducts, as well as by the further "traditional" chemistry of the *E*-vinylperoxy conformer, all still to be explored in detail. Most interestingly, reaction of this *E*-vinylperoxy with NO_2 is expected to quickly yield an hydroxy-carbonylnitrate, a process that to our knowledge is newly characterized here:

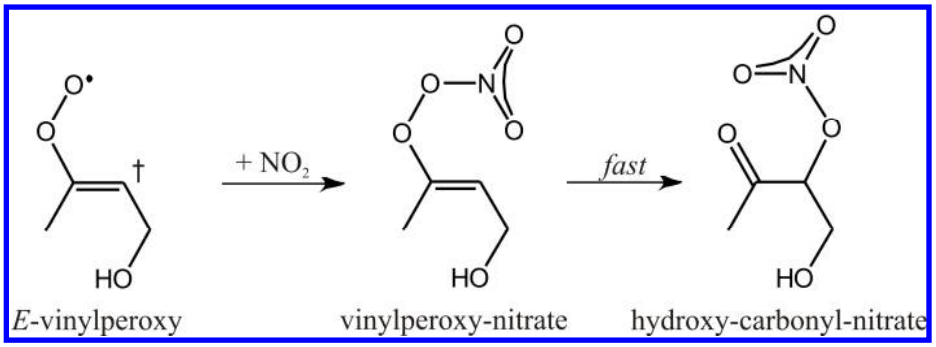

The radical-radical combination of a vinylperoxy with NO_2 leads first to a vinylperoxynitrate. While alkylperoxynitrates, which are stable for only around 20 kcal mol^{-1}, merely redissociate within a fraction of a second,[55] a preliminary investigation revealed that the vinylperoxynitrate proxy $H_2C{=}CHOONO_2$ should readily isomerise over a barrier estimated between 11 and 16 kcal mol^{-1} through a fairly loose TS directly

to a carbonyl-nitrate that is *ca.* 63 kcal mol^{-1} more stable. This newly predicted pathway may contribute substantially to nitrate formation from isoprene. Interestingly, the hydroxy-carbonyl-nitrates expected here are precisely the major carbonyl-nitrates formed in the oxidation of isoprene at high NO[83] and that were recently argued to undergo rapid photolyis.[84]

For Case I, the chemistry following the low-barrier 1,5-H shift of a methyl-hydrogen in the *E*-oxy from HPALD photolysis shows greater potential for OH-recycling. The three or four probable reaction sequences that can be envisaged are expected to result in the net regeneration of 2 up to 4 hydroxyl radicals. These pathways too need to be further examined theoretically in detail and kinetically quantified in future work.

Concerning the reactions of the HPALDs with OH, we can be brief here and refer to a previous paper and its Supporting Information,[21] in which the possible reaction channels and the overall rate constant were discussed in detail, predicting that nearly all channels regenerate OH, including a major route yielding an unsaturated peracid-aldehyde (PACALD), and estimating a total rate coefficient of about 5×10^{-11} cm^3 s^{-1}, as experimentally confirmed by Wolfe et al.[28] The subsequent chemistry of PACALDs was discussed earlier,[21] while the other major products are largely hydroperoxy-carbonyls, of which the generic fate will be addressed briefly below, together with that of similar compounds resulting from the di-HPCARPs.

Similar to the oxy radical photoproducts from HPALDs, the subsequent chemistry of the di-HPCARP radicals still needs to be further elucidated and also quantified kinetically; these investigations are ongoing. It can however be expected that the thermalized di-HPCARPs undergo mainly three competitive reactions at low NO levels,

all three displayed in Figure 6 for Case I: (*i*) a 1,4-H shift of the aldehyde-H to the peroxy function, known for similar cases to face a barrier around 20 - 21 kcal mol^{-1} and therefore to have a rate of order 0.1 s^{-1};[67,85] (*ii*) the traditional reactions with NO and (*iii*) with HO_2. The 1,4-H shift (*i*) results in a chemically activated acyl radical with internal energy 22 - 25 kcal mol^{-1} that promptly eliminates CO, over a barrier of ≤ 7 kcal mol^{-1},[86] after which the unstable α-hydroperoxy-alkyl will spontaneously expel OH[78] to form a di-hydroperoxy-carbonyl compound. Two other possible H-shifts, of the α-hydroperoxy-hydrogens, will result in OH and di-hydroperoxy-di-carbonyls. Reaction (*ii*) of di-HPCARP with NO will yield (besides nitrates) an oxy radical that dissociates over a negligible barrier[48,49] into methylglyoxal and another unstable α-hydroperoxy-alkyl that breaks up immediately in OH and hydroperoxy-acetaldehyde. Finally, a fraction of the reaction (*iii*) of the α-carbonyl-peroxy di-HPCARP with HO_2 should yield OH and the same oxy radical as produced in the NO reaction,[87] while another, likely larger fraction yields a tri-hydroperoxy-carbonyl. Important to note is that Crounse et al. observed hydroperoxy-acetaldehyde and its hydroperoxy-acetone counterpart from the Case II-sequence in yields about 25% of the HPALDs, whereas in the oxidation of fully deuterated isoprene these products were found in yields comparable to the (deuterated) HPALDs, rationalized by the much lower tunneling factor of D- compared to H atoms in the competing 1,4-D/H shifts (*i*).[88] Since reaction (*iii*) is expected to yield also another product besides hydroperoxy-acetaldehyde or -acetone, these observations indicate that the di-HPCARP/HPALD branching ratio following the *Z*-δ-OH-peroxy 1,6-H shifts is at least equal to and likely even larger than the 0.5 : 0.5 adopted above.

Importantly, several of the di-HPCARP reactions can regenerate OH, and all produce hydroperoxy-carbonyls. The latter compounds can react in mainly two ways: 1° reactions with OH, in particular abstractions of α-hydroperoxy-H's or of aldehyde-H's from the α-hydroperoxy-aldehydes, which are both expected to directly recycle the OH; and 2° photolysis, which for α-hydroperoxy-carbonyls should lead to OH re-generation with a high quantum yield. Indeed, as will be detailed in a follow-up article, high-level M06-2X and CC//QC computations show that excited triplet α-hydroperoxy-carbonyls, resulting from fast intersystem crossing of the initially excited singlet states upon ≈ 315-340 nm absorption,[89] decompose within picoseconds over a barrier of only 3.5 - 4.5 kcal mol^{-1} into an acyl radical and an unstable α-hydroperoxyalkyl radical that spontaneously expels OH to form a carbonyl, whereas the concerted H-shift and triplet O_2 elimination via a Norrish II mechanism is over an order of magnitude slower. Again, the net budget of OH from hydroperoxy-carbonyls will be decided by the competition of their photolysis and OH reactions and subsequent chemistry, all still to be fully elucidated and quantified.

Conclusions

In this work, by using much higher levels of theory that (*i*) take into account the crucial London dispersion effects for the H-bonded systems at hand and (*ii*) agree on the barrier heights for the critical H-shifts within <0.3 kcal/mol, we have to a great degree upgraded the quantum-chemical and statistical-kinetics based rate coefficients of the isoprene-peroxy redissociation and isomerisation reactions.

- The peroxy redissociations are shown to be fast enough to allow major interconversion at low NO, though, different from our lower-level earlier findings, full *Z*-δ-OH ⇌ β-

OH-peroxy equilibration within ≤ 5%, is not attained in relevant atmospheric conditions, and in any case the potential $\{[Z\text{-}\delta\text{-OH}]/[\beta\text{-OH}]\}_{eq}$ equilibrium ratios at atmospheric temperatures are only about or below 0.01. The very low steady-state fractions of the *Z*-δ-OH-peroxy radicals that can isomerise lead to (experimentally accessible) bulk-peroxy isomerisation rate "coefficients" that are over two orders of magnitude lower than the rate coefficients of the elementary, isomer-specific 1,6-H shifts of the *Z*-δ-OH-peroxys. The literature on isoprene oxidation should not overlook this critical and major distinction. As revealed by box modeling, the experimental HPALD yield data at varying *T* of Crounse et al.[27] support unequivocally substantial peroxy interconversion as we predicted.

- The isomer-specific rates of the 1,6-H shifts of the *Z*-δ-OH peroxys are found to be of the order of 1 s^{-1}, but, for the reasons above, the bulk peroxy rates k(bulk 1,6-H) = f(*Z*-δ) × k(*Z*-δ 1,6-H) are much lower, of the order of only 0.01 s^{-1} or even less. An important new finding is that the bulk isomerisation rate increases substantially with increasing sink rate k_{tr} of the traditional peroxy removal reactions, because a higher k_{tr} directly reduces the absolute concentration of the majority β-OH-peroxy radicals but has much less influence on [*Z*-δ-OH]. In the recent global modelling work of Taraborrelli et al.,[14] who adopted largely our LIM mechanism, the considerably higher and quasi-equilibrium f(*Z*-δ) fractions of our earlier work[20] were apparently still used, and hence also the dependence of the bulk 1,6-H isomerisation rates on k_{tr} was not accounted for. Their higher f(*Z*-δ) fractions of about 0.067, despite their low k(*Z*-δ 1,6-H) value of 0.14 s^{-1} at 295 K chosen for a best model-fit to the results of Crounse et al.,[27] lead to a k(bulk 1,6-H) of 0.0094 s^{-1}, higher than our present value 0.0070 s^{-1} for k_{tr} = 0.02 s^{-1}.

- The concerted 1,5-H shifts of the majority β-OH-peroxys are found to face very high barriers and hence to be slow, only of the order of 0.001 s^{-1}, in accord with the findings of Crounse et al.,[27] such that they can contribute significantly only at $T \geq 310$ K. These results indicate that the observed OH regeneration in the recent chamber study of Fuchs et al.,[18] at temperatures around 305 K, resulted mainly from the 1,6-H shift of the *Z*-δ-OH-peroxys and subsequent reactions, while direct OH from the 1,5-H shift of the β-OH-peroxys contributed only in a minor way. Further detailed modelling studies could show to what extent LIM1 is quantitatively compatible with these chamber measurements.

- The box-modeled HPALD yields using our explicit LIM1 mechanism and rates are consistent with the experimental results of Crounse et al.,[27] given the respective error margins and taking into account that the 1,6-H shifts result in another, about equally important pathway besides HPALD production. The theoretically characterized second pathway is shown to result in di-hydroperoxy-carbonylperoxy radicals (di-HPCARPs) that are expected to react in several ways, one of which should produce hydroperoxy-acetone and hydroperoxy-acetaldehyde, both observed by Crounse et al.[88] in yields consistent with the above. This second pathway was not considered in the recent modelling work of Taraborrelli et al.[14] such that HPALD production was likely overestimated.

- Based on work still in progress, we expect that the oxy-radical co-product of OH from HPALD photolysis, as well as the di-HPCARP radicals from the second pathway above will both result in considerable, additional, partially delayed OH regeneration.

- Global modeling implementing LIM1 predicts that on average about 30% of the emitted isoprene reacts via the isomerisation routes, which, considering the efficient photolysis of

HPALDs and including the expected secondary OH regeneration above, would put total hydroxyl recycling at a considerably higher percentage.

- As implied above, future work should address in the first place the subsequent mechanisms, kinetics and associated OH-budgets of the oxy radical co-products of HPALD photolysis and of the di-HPCARP radicals, while also the potential contribution to OH recycling of photolysis of bi- and tri-functional hydroperoxide compounds should be closely examined.

- Obviously, the theoretically predicted LIM1 mechanisms need to be confirmed — or disproven — and the derived kinetic coefficients will have to be refined by continued, detailed laboratory studies and chamber investigations of isoprene oxidation under realistic atmospheric conditions.

- Once the LIM1 mechanism will be completed, we intend to verify whether LIM1 implemented in regional and global models is able to close the gap in our understanding between measured OH in the field and atmospheric model calculations of OH, for which there is currently a large disparity. However, meaningful comparisons with the observations must await clarification regarding instrumental artifacts in the FAGE-based measurements of OH, recently reported to be as high as 30-80% in several field campaigns.[19, 90]

- Interestingly, from a fundamental point of view, it is hydrogen bonding — involving energies of only a few kcal mol^{-1} — that ultimately determines the fraction of isoprene-derived peroxy radicals that can undergo the crucial 1,6-H shift, and it is hydrogen atom tunneling that ultimately makes this reaction and the LIM mechanism really important.

AUTHOR INFORMATION

Notes

The authors declare no competing financial interest.

Biographies

Jozef Peeters was born in Antwerp, Belgium in 1941. He took degrees of Licenciate in Chemistry at the University of Leuven, Belgium in 1963 and Master of Arts at the University of Toronto, Canada in 1965. He obtained a Ph.D. in Chemical Sciences at the University of Leuven in 1967, with Prof. Adolphe Van Tiggelen. Since 1971, he was appointed successively as lecturer, professor and full professor at the University of Leuven, where he is now professor emeritus. He founded the reaction kinetics group at the University of Leuven in the early seventies. His early interests were mainly focused on highly reactive, small radicals in combustion chemistry, such as methyl, singlet methylene and ketenyl, of which, with his group, he elucidated the reaction mechanisms and quantified the kinetics in low-pressure flames and later in flow reactor systems. Since the late eighties, he also made use of laser-based techniques such as laser photodissociation - laser induced fluorescence to investigate the reaction kinetics of CF and CF_2 radicals, and developed laser photodissociation - chemiluminescence methods to

determine kinetic coefficients of C_2H radical reactions. Since the mid-nineties, his research interests gradually went more to the atmospheric chemistry of larger biogenic compounds and the liquid-phase autoxidation chemistry of larger hydrocarbons, striving to unravel the rich but complex peroxy radical chemistry involved by theoretical means. Jozef Peeters taught six courses at the University of Leuven, ranging from *Principles of General Chemistry* to *Advanced Techniques in Physical Chemistry*; he also had the pleasure and privilege of guiding 45 graduate students to their Ph.D.

Jean-François Müller, born in 1965 in Uccle, Belgium, obtained his Master Degree (Licence en Physique) from the University of Brussels. His PhD, conducted at the same University under the supervision of Prof. Guy Brasseur, gave him the opportunity to work on atmospheric chemistry modeling at NCAR in the United States and at the Belgian Institute for Space Aeronomy (BISA), where he works since 1988. His interests include the modeling of biogenic emissions, the oxidation mechanisms of key biogenic volatile organic compounds, the formation of secondary organic aerosols, and the use of

both suborbital and satellite data to evaluate and constrain the emissions of reactive tropospheric compounds. He is head of the tropospheric chemistry modeling section at BISA.

Trissevgeni Stavrakou, born in 1969 in Athens, Greece, graduated in 1992 at the Faculty of Sciences of the University of Thessaloniki in Greece. She received her PhD degree in Mathematical Physics from the University of Marseilles II in 1997. Since 2001, she works in the field of atmospheric chemistry and emission modeling at the Belgian Institute for Space Aeronomy. She has in particular developed and utilized inverse modeling techniques for retrieving reactive gas emissions from the combination of mathematical models with ground-based and satellite measurements.

Vinh Son Nguyen, born in 1979 in Hanoi, Vietnam, graduated in 2001 and obtained his M.Sc. in Chemistry from Hanoi National University of Education. He received his Ph.D. degree in Chemistry from the Katholieke Universiteit Leuven (KU Leuven), Belgium for work on computational study of materials for chemical hydrogen storage. He is currently a postdoctoral fellow in Division of Chemical Physics and Physical Chemistry, KU Leuven and his research interests involve theoretical studies on chemical reaction mechanisms of gas phase molecules in the atmospheric chemistry.

Acknowledgement

This research was sponsored by the Belgian Science Policy Office (BELSPO) under the contracts SD/AT/03A and -B (project IBOOT) and SD/CS/05A (project BIOSOA) in the frame of the Science for Sustainable Development program.

Supporting Information Available: Extensive and detailed supplementary information on all aspects of this work is available. This material is available free of charge via the Internet at http://pubs.acs.org.

Table 1. Observed and modeled production rates (pptv/min) of isoprene oxidation products in the experiments of Crounse et al.[27] Model results obtained when ignoring the interconversion of isoprene peroxys are indicated within parentheses.

	MVK + MACR		ISOPNO2		ISOPOOH		HPALD	
	obs.	LIM1	**obs.**	LIM1	**obs.**	LIM1	**obs.**	LIM1
Exp. # 1 (295.2 K)	**7.53**	6.77 (6.38)	**0.53**	0.56 (0.62)	**4.27**	4.13 (4.10)	**1.02**	1.85 (1.83)
Exp. # 2 (310.2 K)	**5.31**	6.96 (8.01)	**0.36**	0.47 (0.66)	**3.78**	3.94 (4.43)	**2.78**	4.78 (2.21)
Exp. # 3 (318.2 K)	**4.76**	7.31 (10.1)	**0.16**	0.39 (0.68)	**3.10**	3.62 (4.66)	**4.06**	7.47 (2.62)

Figure Captions

Figure 1. LIM1 reaction scheme of OH-initiated oxidation of isoprene under low-NO conditions for initial $HOCH_2C(CH_3)CHCH_2$ hydroxy-isoprenyl adducts (Case I). Peroxy isomerisation reactions and subsequent chemistry. Rate constants shown are at 298 K.

Figure 2. LIM1 reaction scheme of OH-initiated oxidation of isoprene under low-NO conditions for initial $CH_2C(CH_3)CHCH_2OH$ hydroxy-isoprenyl adducts (Case II). Peroxy isomerisation reactions and subsequent chemistry. Rate constants shown are at 298 K.

Figure 3. Potential energy surface (PES) of 1,6-H shift isomerisation of most stable conformer of *Z*-δ-OH-peroxy radical, *Z*-$HOCH_2$-$C(CH_3)$=CH-$CH_2OO^{\bullet}$. Energies at CCSD(T)/aug-cc-PVTZ **//** QCISD/6-311G(d,p) level of theory, including ZPVE at M06-2X/311++G(3df,2p) level. Reactant, transition state and product are hydrogen-bonded.

Figure 4. Isomerisation (1,6 and 1,5 H-shift) yields in the oxidation of isoprene by OH at 295 and 303 K, and yields of traditional (β-OH-RO_2 and δ-OH-RO_2) peroxy reaction products, as functions of the traditional sink rate (k_{tr}) of isoprene peroxys.

Figure 5. Potential energy surface (PES) of O_2 addition to *Z,Z′* OH-allylic product of 1,6-H shift isomerisation (Case I, see Figure 3) forming a 1st peroxy and 2nd peroxy, and subsequent chemistry; M06-2X/311++G(3df,2p) level of theory (including ZPVE).

Figure 6. Expected subsequent chemistry at low NO of di-hydroperoxy-carbonyl-peroxy radicals (di-HPCARP) resulting from 2nd peroxy (Case I, see Figure 5).

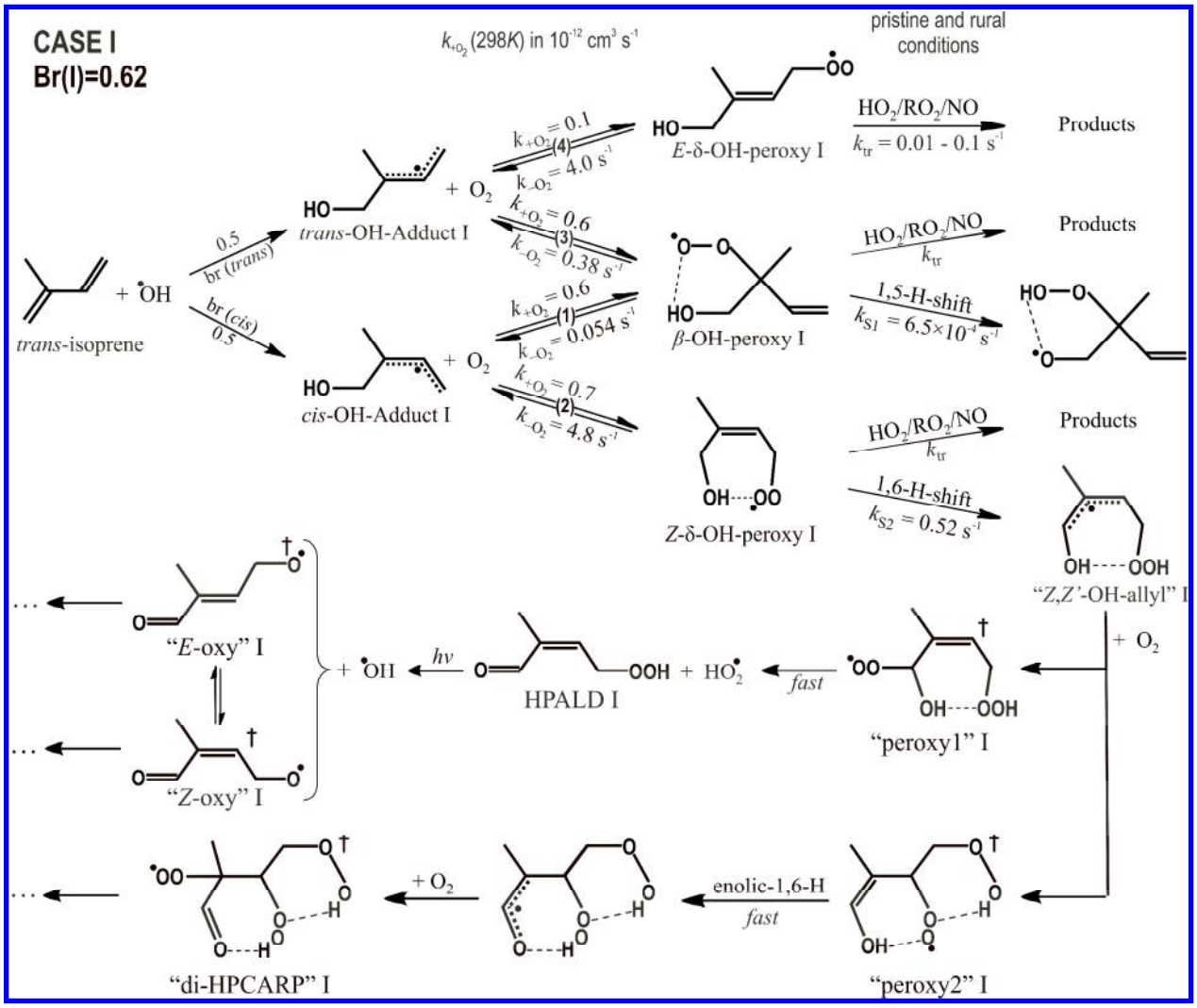
CASE I
Br(I)=0.62
k_{+O_2} (298K) in 10^{-12} cm^3 s^{-1}
pristine and rural conditions
trans-isoprene
+ OH
0.5 br (trans)
0.5 br (cis)
trans-OH-Adduct I
cis-OH-Adduct I
+ O2
k+O2 = 0.1 (4) k-O2 = 4.0 s-1
k+O2 = 0.6 (3) k-O2 = 0.38 s-1
k+O2 = 0.6 (1) k-O2 = 0.054 s-1
k+O2 = 0.7 (2) k-O2 = 4.8 s-1
E-δ-OH-peroxy I
β-OH-peroxy I
Z-δ-OH-peroxy I
HO2/RO2/NO ktr = 0.01 - 0.1 s-1
HO2/RO2/NO ktr
1,5-H-shift kS1 = 6.5×10-4 s-1
1,6-H-shift kS2 = 0.52 s-1
Products
"Z,Z'-OH-allyl" I
+ O2
"peroxy1" I
"peroxy2" I
enolic-1,6-H fast
+ O2
"di-HPCARP" I
"E-oxy" I
"Z-oxy" I
+ OH
hv
HPALD I
+ HO2
fast

Figure 1.

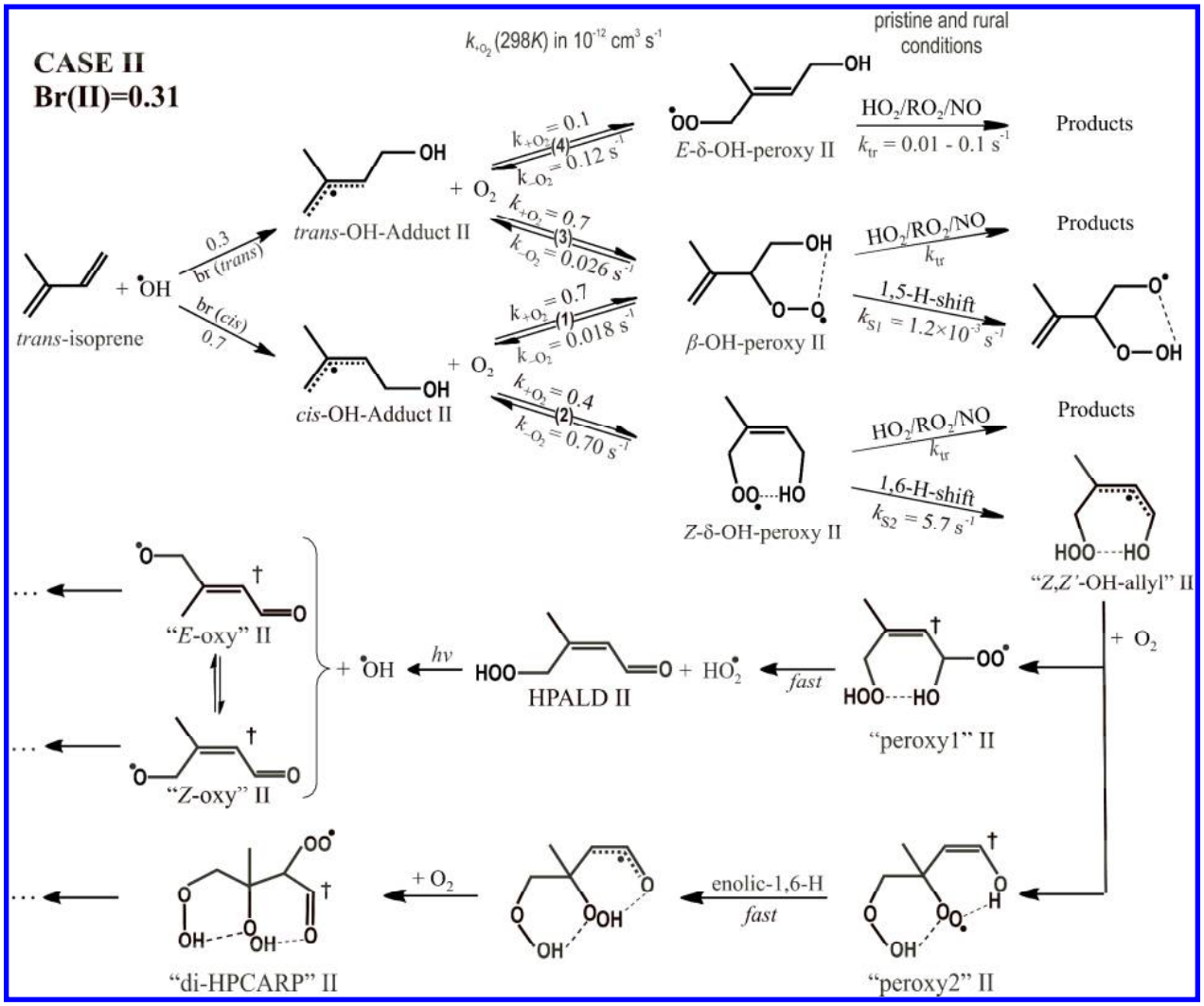
CASE II
Br(II)=0.31
k_{+O_2}(298K) in 10^{-12} cm^3 s^{-1}
pristine and rural conditions
trans-isoprene
+ OH
0.3
br (trans)
br (cis)
0.7
trans-OH-Adduct II
cis-OH-Adduct II
+ O2
k_{+O_2} = 0.1
(4)
k_{-O_2} = 0.12 s^{-1}
k_{+O_2} = 0.7
(3)
k_{-O_2} = 0.026 s^{-1}
k_{+O_2} = 0.7
(1)
k_{-O_2} = 0.018 s^{-1}
k_{+O_2} = 0.4
(2)
k_{-O_2} = 0.70 s^{-1}
E-δ-OH-peroxy II
β-OH-peroxy II
Z-δ-OH-peroxy II
HO2/RO2/NO
k_{tr} = 0.01 - 0.1 s^{-1}
1,5-H-shift
k_{S1} = 1.2×10^{-3} s^{-1}
1,6-H-shift
k_{S2} = 5.7 s^{-1}
Products
"Z,Z'-OH-allyl" II
"E-oxy" II
"Z-oxy" II
hv
HPALD II
+ HO2
fast
"peroxy1" II
"peroxy2" II
enolic-1,6-H
fast
"di-HPCARP" II

Figure 2.

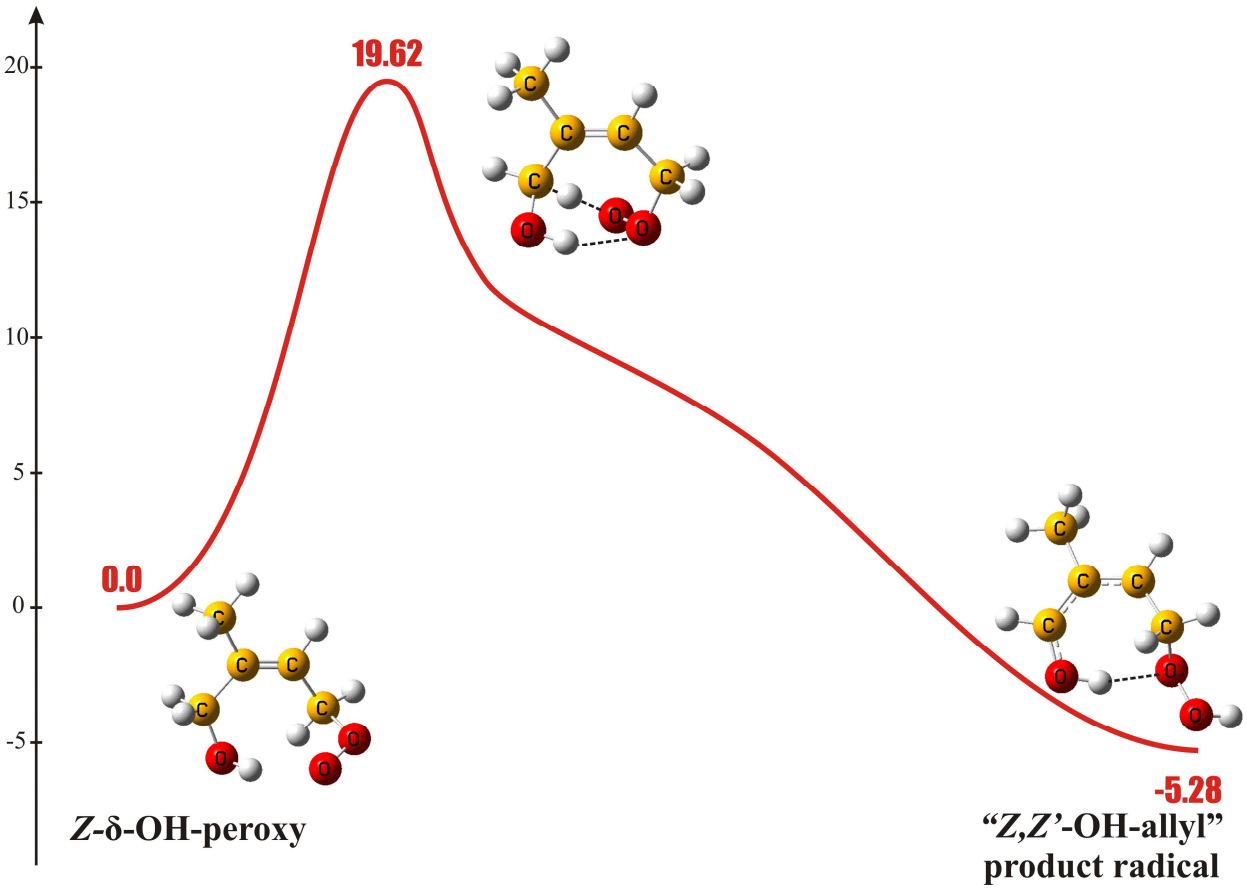
20
15
10
5
0
-5
19.62
0.0
-5.28
Z-δ-OH-peroxy
"Z,Z'-OH-allyl"
product radical

Figure 3.

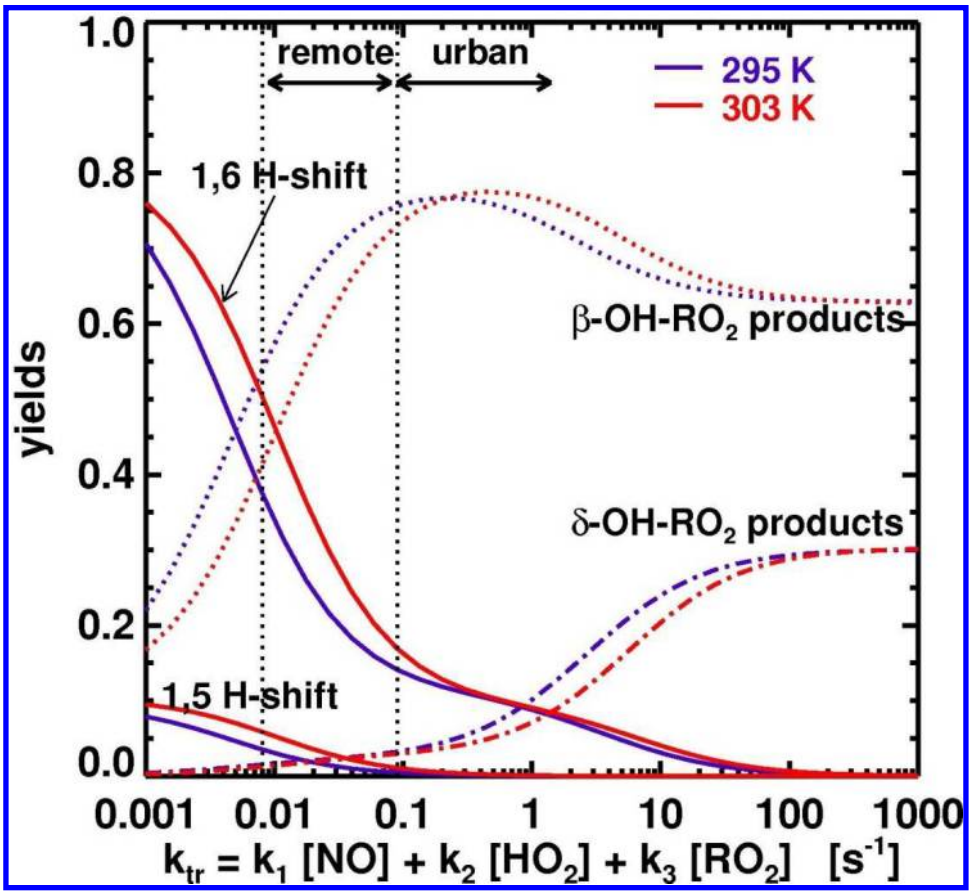
1.0
0.8
0.6
0.4
0.2
0.0
yields
remote
urban
295 K
303 K
1,6 H-shift
β-OH-RO2 products
δ-OH-RO2 products
1,5 H-shift
0.001
0.01
0.1
1
10
100
1000
ktr = k1 [NO] + k2 [HO2] + k3 [RO2] [s-1]

Figure 4.

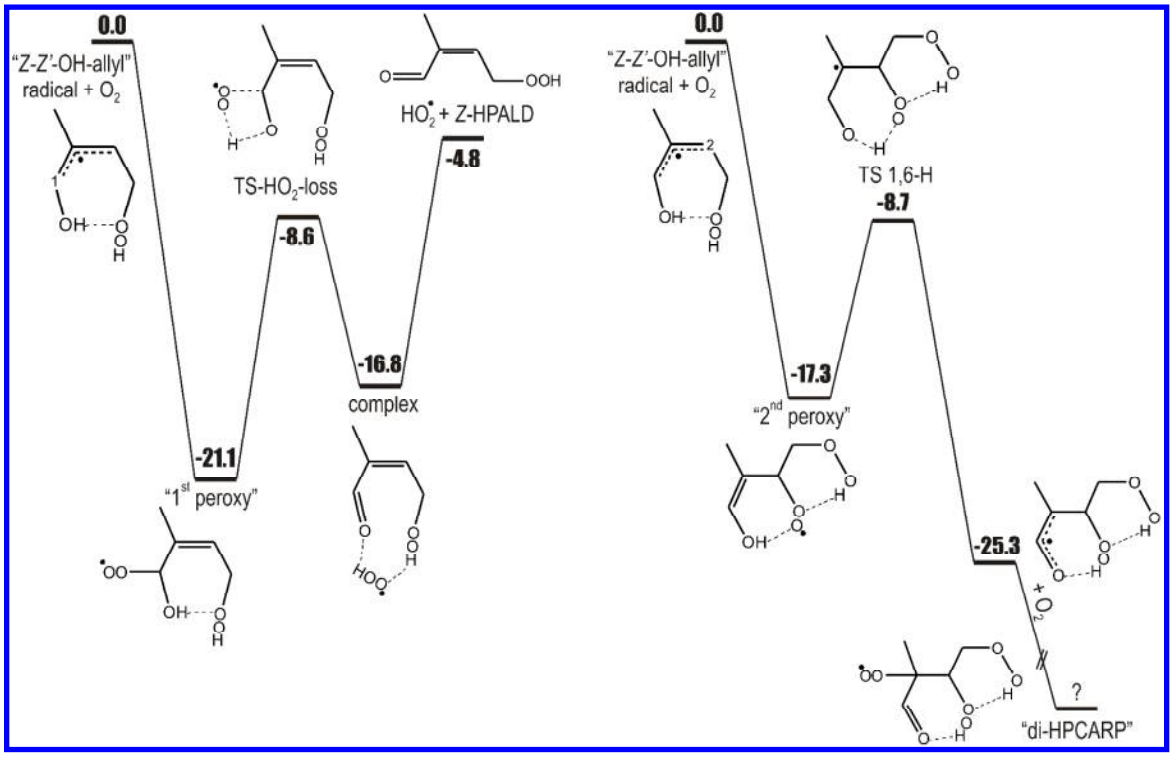
0.0
"Z-Z'-OH-allyl" radical + O_2
-21.1
"1st peroxy"
TS-HO_2-loss
-8.6
$HO_2^{\bullet}$ + Z-HPALD
-4.8
-16.8
complex
0.0
"Z-Z'-OH-allyl" radical + O_2
-17.3
"2nd peroxy"
TS 1,6-H
-8.7
-25.3
+ O_2
?
"di-HPCARP"

Figure 5.

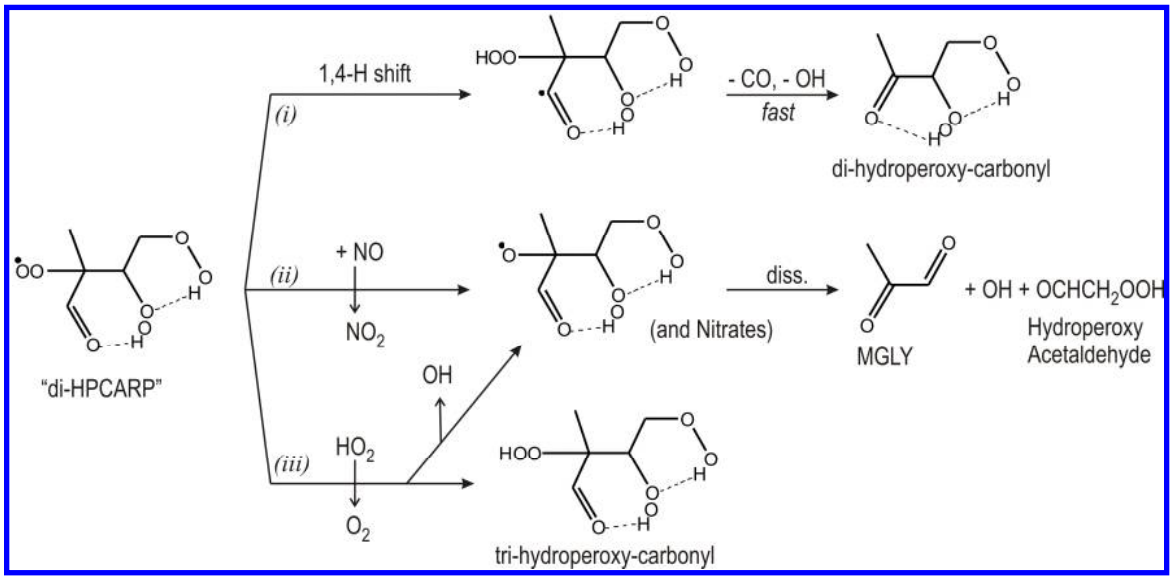
1,4-H shift
(i)
HOO
- CO, - OH
fast
di-hydroperoxy-carbonyl
"di-HPCARP"
(ii)
+ NO
NO2
(and Nitrates)
diss.
MGLY
+ OH + OCHCH2OOH
Hydroperoxy
Acetaldehyde
(iii)
HO2
O2
OH
tri-hydroperoxy-carbonyl

Figure 6.

References

(1) Goldstein, A. H.; Galbally, I. E. Known and unexplored organic constituents in the earth's atmosphere, *Environ. Sci. Technol.* **2007**, *41*, 1514-1521.

(2) Laothawornkitkul, J.; Taylor, J. E.; Paul, N. D.; Hewitt, C. N. Biogenic volatile organic compounds in the Earth system, *New Phytologist* **2009**, *183*, 27-51.

(3) Guenther, A. B.; Jiang, X.; Heald, C. L.; Sakulyanontvittaya, T.; Duhl, T.; Emmons, L. K.; Wang, X. The Model of Emissions of Gases and Aerosols from Nature version 2.1 (MEGAN2.1): an extended and updated framework for modeling biogenic emissions, *Geosci. Model. Dev.* **2012**, *5*, 1471-1492.

(4) Paulot, F.; Crounse, J. D.; Kjaergaard, H. G.; Kürten, A.; Clair, J. M. S.; Seinfeld, J. H.; Wennberg, P. O. Unexpected Epoxide Formation in the Gas-Phase Photooxidation of Isoprene, *Science* **2009**, *325*, 730-733.

(5) Henze, D. K.; Seinfeld, J. H. Global secondary organic aerosol from isoprene oxidation Geophys, *Res. Lett.* **2006**, *33*, L09812, doi:10.1029/2006GL025976.

(6) Lin, G.; Penner, J. E.; Sillman, S.; Taraborrelli, D. & Lelieveld, J. Global modeling of SOA formation from dicarbonyls, epoxides, organic nitrates and peroxides, *Atmos. Chem. Phys.* **2012**, *12*, 4743-4774.

(7) Carslaw, N.; Creasey, D. J.; Harrison, D.; Heard, D. E.; Hunter, M. C.; Jacobs, P. J.; Jenkin, M. E.; Lee, J. D.; Lewis, A. C.; Pilling, M. J.; et al. OH and HO_2 radical chemistry in a forested region of north-western Greece, *Atmos. Environ.* **2001**, *35*, 4725-4737.

(8) Tan, D.; Faloona, I.; Simpas, J. B.; Brune, W.; Shepson, P. B.; Couch, T. L.; Sumner, A. L.; Carroll, M. A.; Thornberry, T.; Apel, E.; Riemer, D.; Stockwell, W. HOx

budget in a deciduous forest: result from the PROPHET summer 1998 campaign, *J. Geophys. Res.* **2001**, *106*, 24407-24427.

(9) Ren, X. R.; Olson, J. R.; Crawford, J. H.; Brune, W. H.; Mao, J. Q.; Long, R. B.; Chen, Z.; Chen, G.; Avery, M. A.; Sachse, G. W.; et al., HOx chemistry during INTEX-A: Observation, model calculation, and comparison with previous studies, *J. Geophys. Res.* **2008**, *113*, D05310.

(10) Lelieveld, J.; Butler, T. M.; Crowley, J. N.; Dillon, T. J.; Fischer, H.; Ganzeveld, L.; Harder, H.; Lawrence, M. G.; Martinez, M.; Taraborrelli, D.; Williams, J. Atmospheric oxidation capacity sustained by a tropical forest, *Nature* **2008**, *452*, 737-740.

(11) Hofzumahaus, A.; Rohrer, F.; Lu, K.; Bohn, B.; Brauers, T.; Chang, C.-C.; Fuchs, H.; Holland, F.; Kita, K.; Kondo, Y., et al., Amplified Trace Gas Removal in the Troposphere, *Science* **2009**, *324*, 1702-1704.

(12) Whalley, L. K.; Edwards, P. M.; Furneaux, K. L.; Goddard, A.; Ingham, T.; Evans, M. J.; Stone, D.; Hopkins, J. R.; Jones, C. E.; Karunaharan, A.; et al., Quantifying the magnitude of a missing hydroxyl radical source in a tropical rainforest, *Atmos. Chem. Phys.* **2011**, *11*, 7223-7233.

(13) Stone, D.; Evans, M. J.; Edwards, P. M.; Commane, R.; Ingham, T.; Rickard, A. R.; Brookes, D. M.; Hopkins, J.; Leigh, R. J.; Lewis, A. C.; et al., Isoprene oxidation mechanisms: Measurements and modeling of OH and HO2 over a South-East Asian tropical rainforest during the OP3 field campaign, *Atmos. Chem. Phys.* **2011**, *11*, 6749-6771.

(14) Taraborrelli, D.; Lawrence, M. G.; Crowley, J. N.; Dillon, T. J.; Gromov, S.; Grosz, C. B. M.; Vereecken, L.; Lelieveld, J. Hydroxyl radical buffered by isoprene oxidation over tropical forests, *Nature Geosci*. **2012**, *5*, 190-193.

(15) Stone, D.; Whalley, L. K.; Heard, D. E. Tropospheric OH and HO2 radicals: field measurements and model comparisons, *Chem. Soc. Rev.*, **2012**, *41*, 6348-6404.

(16) Lu, K. D.; Rohrer, F.; Holland, F.; Fuchs, H.; Bohn, B.; Brauers, T.; Chang, C. C.; Hüseler, R.; Hu, M.; Kita, K., et al., Observation and modelling of OH and HO2 concentrations in the Pearl River Delta 2006: A missing OH source in a VOC rich atmosphere, *Atmos. Chem. Phys.* **2012**, *12*, 1541-1569.

(17) Lu, K. D.; Hofzumahaus, A.; Holland, F.; Bohn, B.; Brauers, T.; Fuchs, H.; Hu, M.; Hüseler, R.; Kondo, K. K. A.; Li, X.; et al., Missing OH source in a suburban environment near Beijing: observed and modelled OH and HO_2 concentrations in summer 2006, *Atmos. Chem. Phys.* **2013**, 13, 1057-1080.

(18) Fuchs, H.; Hofzumahaus, A.; Rohrer, F.; Brauers, T.; Dorn, H.-P.; Häseler, R.; Holland, F.; Kaminski, M.; Li, X.; Lu, K.; Nehr, S.; Tillmann, R.; Wegener, R.; Wahner, A. Experimental evidence for efficient hydroxyl radical regeneration in isoprene oxidation, *Nat. Geosci.* **2013**, *6*, 1023-1026.

(19) Mao, J.; Ren, X.; Zhang, L.; Van Duin, D. M.; Cohen, R. C.; Park, J.-H.; Goldstein, A. H.; Paulot, F.; Beaver, M. R.; Crounse, J. D.; et al., Insights into hydroxyl measurements and atmospheric oxidation in a California forest, *Atmos. Chem. Phys.*, **2012**, *12*, 8009–8020.

(20) Peeters, J.; Nguyen, T. L.; Vereecken, L. HOx radical regeneration in the oxidation of isoprene, *Phys. Chem. Chem. Phys.* **2009**, *11*, 5935-5939.

(21) Peeters, J.; Müller, J.-F. HOx radical regeneration in isoprene oxidation via peroxy radical isomerisations. II: experimental evidence and global impact, *Phys. Chem. Chem. Phys.* **2010**, *12*, 14227-14235.

(22) Nguyen, T. L.; Peeters, J.; Vereecken, L. HOx Regeneration in the Oxidation of Isoprene III: Theoretical Study of the key Isomerisation of the *Z*-δ-hydroxy-peroxy Isoprene Radicals, *Chem. Phys. Chem.* **2010**, *11*, 3996-4001.

(23) Da Silva, G.; Graham, C.; Wang, Z.-F. Unimolecular beta-hydroxyperoxy radical decomposition with OH recycling in the photochemical oxidation of isoprene, *Environ. Sci. Technol.* **2010**, *44*, 250-256.

(24) Stavrakou, T.; Peeters, J.; Müller, J.-F. Improved global modelling of HOx recycling in isoprene oxidation: evaluation against the GABRIEL and INTEX-A aircraft campaign measurements, *Atmos. Chem. Phys.* **2010**, *10*, 9863-9878.

(25) Archibald, A.; Cooke, M. C.; Utembe, S. R.; Shallcross, D.; Derwent, R. G. & Jenkin, M. E. Impacts of mechanistic changes on HOx formation and recycling in the oxidation of isoprene, *Atmos. Chem. Phys.* **2010**, *10*, 8097-8118.

(26) Archibald, A. T.; Levine, N. L.; Abraham, N. L.; Cooke, M. C.; Edwards, P. M.; Heard, D. E.; Jenkin, M. E.; Karunaharan, A.; Pike, R. C.; Monks, P. S.; et al., Impacts of HOx regeneration and recycling in the oxidation of isoprene: Consequences for the composition of past, present and future atmospheres, *Geophys. Res. Lett.* **2011**, *38*, L05804.

(27) Crounse, J. D.; Paulot, F.; Kjaergaard, H. G.; Wennberg, P. O. Peroxy radical isomerization in the oxidation of isoprene, *Phys. Chem. Chem. Phys.* **2011,** *13*, 13607-13613.

(28) Wolfe, G. M.; Crounse, J. D.; Parrish, J. D.; St Clair, J. M.; Beaver, M. R.; Paulot, F.; Yoon, T. P.; Wennberg, P. O.; Keutsch, F. N. Photolysis, OH reactivity and ozone reactivity of a proxy for isoprene-derived hydroperoxyenals (HPALDs), *Phys. Chem. Chem. Phys.* **2012**, *14*, 7276-7286.

(29) Peeters, J.; Vereecken, L.; Fantechi, G. The detailed mechanism of the OH-initiated atmospheric oxidation of alpha-pinene: a theoretical study, *Phys. Chem. Chem. Phys.* **2001**, *3*, 5489-5504.

(30) Fantechi, G.; Vereecken, L.; Peeters, J. The OH-initiated atmospheric oxidation of pinonaldehyde: Detailed theoretical study and mechanism construction, *Phys. Chem. Chem. Phys.* **2002**, *4*, 5795-5805.

(31) Ceulemans, K. ; Compernolle, S.; Peeters, J.; Müller, J.-F. Evaluation of a detailed model of secondary organic aerosol formation from α-pinene against dark ozonolysis experiments, *Atmospheric Environment* **2010**, *44*, 5434-5442.

(32) Ceulemans, K. ; Compernolle, S.; Müller, J.-F. Parameterising secondary organic aerosol from α-pinene using a detailed oxidation and aerosol formation model, *Atmos. Chem. Phys.* **2012**, *12*, 5343-5366.

(33) Vereecken, L.; Peeters, J. Nontraditional (per)oxy ring-closure paths in the atmospheric oxidation of isoprene and monoterpenes, *J. Phys. Chem. A* **2004**, *108*, 5197-5204.

(34) Hermans, I.; Müller, J.-F.; Nguyen, T.; Jacobs, P.; Peeters, J. Kinetics of alpha-Hydroxy-alkylperoxyl Radicals in Oxidation Processes. HO_2-Initiated Oxidation of Ketones/Aldehydes near the Tropopause, *J. Phys. Chem. A* **2005**, *109*, 4303-4311.

(35) Vereecken, L.; Müller, J.-F.; Peeters, J. Low-volatility poly-oxygenates in the OH-initiated atmospheric oxidation of -pinene: impact of non-traditional peroxyl radical chemistry, *Phys. Chem. Chem. Phys.* **2007**, *9*, 5241-5248.

(36) Zhao, Y.; Truhlar, D. G. The M06 suite of density functionals for main group thermochemistry, thermochemical kinetics, noncovalent interactions, excited states, and transition elements: two new functionals and systematic testing of four M06-class functionals and 12 other functionals, *Theor. Chem. Account* **2008**, *120*, 215-241.

(37) Frisch, M. J. ; Pople, J. A. ; Binkley, J. S. Self-Consistent Molecular Orbital Methods. 25. Supplementary Functions for Gaussian Basis Sets, *J. Chem. Phys.* **1984**, *80*, 3265-3269.

(38) Curtiss, L. A.; Raghavachari, K.; Redfern C.; Rassolov, V.; Pople, J. A. Gaussian-3 (G3) theory for molecules containing first and second-row atoms, *J. Chem. Phys.* **1998**, *109*, 7764.

(39) Pople, J. A.; Head-Gordon, M.; Raghavachari K. Quadratic Configuration Interaction. A general technique for determining electron correlation energies, *J. Chem. Phys.* **1987**, *87* ,5968.

(40) Raghavachari, K.; Trucks, G. W.; Pople, J. A.; Head-Gordon, M. A Fifth Order Perturbation Comparison of Electron Correlation Theories, *Chem. Phys. Lett.* **1989**, *157*, 479-483.

(41) Kendall, R. A.; Dunning Jr. T. H.; Harrison, R. J. Electron affinities of the first-row atoms revisited. Systematic basis sets and wave functions, *J. Chem. Phys.* **1992**, *96*, 6796-806.

(42) Woon, D. E.; Dunning, Jr. T. H. Gaussian-basis sets for use in correlated molecular calculations. 3. The atoms aluminum through argon, *J. Chem. Phys.* **1993**, *98*, 1358-1371.

(43) Gaussian 09, Revision D.01, Frisch, M. J.; et al., Gaussian, Inc., Wallingford CT, 2009.

(44) MOLPRO is a package of ab initio program written by Werner, H.-J.; Knowles, P. L.; Knizia, G.; Manby, F. R.; Schütz, M.; Celani, P.; Korona, T.; Lindh. R.; Mitrushenkov, A.; Rauhut, G.; et al.

(45) Vereecken, L.; Peeters, J. The 1,5-H-shift in 1-butoxy: A case study in the rigorous implementation of transition state theory for a multirotamer system, *J. Chem. Phys.* **2003**, *119*, 5159-5170.

(46) Zhang, F.; Dibble, T. S. Impact of tunneling on hydrogen-migration of the n-propylperoxy radical, *Phys. Chem. Chem. Phys.* **2011**, *13*, 17969-17977.

(47) Peeters, J.; Boullart, W., Pultau, V. Vanderberk, S.; Vereecken, L. Structure-activity relationship for the addition of OH to (poly)alkenes : Site-specific and total rate constans, *J. Phys. Chem. A* **2007**, *111*, 1618-1631.

(48) Peeters, J.; Fantechi, G.; Vereecken, L. A generalized structure-activity relationship for the decomposition of (substituted) alkoxy radicals, *J. Atmos. Chem.* **2004**, *48*, 59-80.

(49) Vereecken, L.; Peeters, J. Decomposition of substituted alkoxy radicals—part I: a generalized structure-activity relationship for reaction barrier heights, *Phys. Chem. Chem. Phys.* **2009**, *11*, 9062-9074.

(50) Vereecken, L.; Peeters, J. A structure-activity relationship for the rate coefficient of H-migration in substituted alkoxy radicals, *Phys. Chem. Chem. Phys.* **2010**, *11*, 12608-12620.

(51) Peeters, J.; Boullart, W.; Hoeymissen, J. V. in *Proceedings of Eurotrac Symposium'94*, ed. P. M. Borrell, et al., SPB Academic Publishers, The Hague, **1994**, p. 110.

(52) Park, J.; Jongsma, C. G.; Zhang, R.; North, S. W. OH/OD Initiated Oxidation of Isoprene in the Presence of O_2 and NO, *J. Phys. Chem. A* **2004**, *108*, 10688-10697.

(53) Lightfoot, P. D.; Cox, R. A.; Crowley, J. N.; Destriau, M.; Hayman, G. D.; Jenkin, M. E.; Moortgat, G. K.; Zabel, F. Organic peroxy radicals : kinetics, spectroscopy and tropospheric chemistry, *Atmospheric Environment* **1992**, *26A*, 1805-1961.

(54) Orlando, J. J. ; Tyndall, G. S. Laboratory studies of organic peroxy radical chemistry: an overview with emphasis on recent issues of atmospheric significance, *Chem. Soc. Rev.* **2012**, *41*, 6294-6317.

(55) Atkinson, R.; Baulch, D. L.; Cox, R. A.; Crowley, J. N.; Hampson, R. F.; Hynes, R. G.; Jenkin, M. E.; Rossi, M. J.; Troe, J.: Evaluated kinetic and photochemical data for atmospheric chemistry: Volume II - gas phase reactions of organic species, *Atmos. Chem. Phys.* **2006**, *6*, 3625-4055.

(56) Boyd, A.; Flaud, P.-M.; Daugey, N.; Lesclaux, R. Rate Constants for RO_2 + HO_2 Reactions Measured under a Large Excess of HO_2, *J. Phys. Chem. A* **2003**, *107*, 818-821.

(57) Liu, Y. J.; Herdlinger-Blatt, I.; McKinney, K. A.; Martin, S. T. Production of methyl vinyl ketone and methacrolein via the hydroperoxyl pathway of isoprene oxidation, *Atmos. Chem. Phys*. **2013**, *13*, 5715-5730.

(58) Boyd, A. A.;Lesclaux, R.; Jenkin, M. E.; Wallington, T. J. A Spectroscopic, Kinetic, and Product Study of the $(CH_3)_2C(OH)CH_2O_2$ Radical Self Reaction and Reaction with HO_2, *J. Phys. Chem.* **1996**, *100*, 6594.

(59) Jenkin, M. E.; Boyd, A. A.; Lesclaux, R. Peroxy Radical Kinetics Resulting from the OH-Initiated Oxidation of 1,3-Butadiene, 2,3-Dimethyl-1,3-Butadiene and Isoprene, *J. Atmos. Chem.* **1998**, *29*, 267-298.

(60) Lei, W.; Zhang, R. Theoretical Study of Hydroxyisoprene Alkoxy Radicals and Their Decomposition Pathways *J. Phys. Chem. A* **2001**, *105*, 3808.

(61) Greenwald, E. E.; North, S. W.; Georgievskii, Y.; Klippenstein, S. J. A Two Transition State Model for Radical−Molecule Reactions: Applications to Isomeric Branching in the OH−Isoprene Reaction, *J. Phys. Chem. A* **2007**, *111*, 5582-5592

(62) Dibble, T. S. Isomerization of OH-isoprene adducts and hydroxyalkoxy isoprene radicals, *J. Phys. Chem. A* **2002**, *106*, 6643-6650.

(63) *IUPAC subcommittee for Gas Kinetic Data Evaluation: HOx + isoprene datasheet*: http://iupac.pole-ether.fr/datasheets/pdf/HOx_VOC8_HO_CH2C(CH3)CHCH2(isoprene).pdf

(64) Ghosh, B. ; Bugarin, A.; Connell, B. T. ; North, S. W. Isomer-Selective Study of the OH-Initiated Oxidation of Isoprene in the Presence of O_2 and NO: 2. The Major OH Addition Channel, *J. Phys. Chem. A* **2010**, *114*, 2553-2560.

(65) Zhang, D.; Zhang, R. Y.; Church, C.; North, S. W. Experimental study of hydroxyalkyl peroxy radicals from OH-initiated reactions of isoprene, *Chem. Phys. Lett.* **2001**, *343*, 49.

(66) Koch, R.; Siese, M.; Fittschen, C.; Zetzsch, C. In a contribution to the *EUROTRAC subproject LACTOZ*; Fraunhofer Publica: Germany, 1995; p 268.

(67) Asatryan, R.; da Silva, G.; Bozzelli, J. W. Quantum Chemical Study of the Acrolein (CH_2CHO) + OH + O_2 Reactions, *J. Phys. Chem. A* **2010**, *114*, 8302-8311

(68) Pfeifle, M.; Olzmann, M. Consecutive Chemical Activation Steps in the OH-Initiated Atmospheric Degradation of Isoprene: An Analysis with Coupled Master Equations, *Int. J. Chem. Kinet.* **2014**, 46, 231-244.

(69) Coote, M. L.; Collins, M. A.; Radom, L. Calculation of accurate imaginary frequencies and tunneling coefficients for hydrogen abstraction reactions using IRCmax, *Mol. Phys.* **2003**, *101*, 1329-1338.

(70) Johnson , R. D., III Computational Chemistry Comparison and Benchmark Database, version 14; National Institute of Standards and Technology: Gaithersburg, MD; http://cccbdb.nist.gov. Accessed February 9, 2010.

(71) Simon, L.; Goodman, J. M. How reliable are DFT transition structures? Comparison of GGA, hybrid-meta-GGA and meta-GGA functionals, *Org. Biomol. Chem.* **2011**, *9*, 689.

(72) Pilling, M. J. Reactions of Hydrocarbon Radicals and Biradicals, *J. Phys. Chem. A* **2013**, *117*, 3697-3717

(73) Taraborrelli, D.; Lawrence, M. G.; Butler, T. M.; Sander, R.; Lelieveld, J. Mainz Isoprene Mechanism 2 (MIM2): an isoprene oxidation mechanism for regional and global atmospheric modelling, *Atmos. Chem. Phys.*, **2009**, *9*, 2751-2777.

(74) Stavrakou, T.; Müller, J.-F.; Peeters, J.; Razavi, A.; Clarisse, L.; Clerbaux, C.; Coheur, P.-F.; Hurtmans, D.; De Mazière, M.; Vigouroux, C. *et al.* Satellite evidence for

a large source of formic acid from boreal and tropical forests, *Nature Geosci.* **2012**, *5*, 26-30.

(75) Cocker III, D. R.; Flagan, R. C.; Seinfeld, J. H. State-of-the-art chamber facility for studying atmospheric aerosol chemistry, *Environ. Sci. Technol*. **2001**, *35*, 2594-2601.

(76) Welz, O.; Klippenstein, S. J.; Harding, L. B.; Taatjes, C. A.; Zador, J. Unconventional Peroxy Chemistry in Alcohol Oxidation: The Water Elimination Pathway, *J. Phys. Chem. Lett.* **2013**, *4*, 350-354.

(77) Peeters, J.; Nguyen, T. L. Unusually fast 1,6-H shifts of enolic hydrogens in peroxy radicals: formation of the first-generation C2 and C3 carbonyls in the oxidation of isoprene, *J. Phys. Chem. A* **2012**, *116*, 6134-6141.

(78) Vereecken, L.; Nguyen, T. L.; Hermans, I.; Peeters, J. Computational study of the stability of α-hydroperoxyl- or α-alkylperoxyl substituted alkyl radicals, *Chem. Phys. Lett.* **2004**; *393*, 432-436.

(79) Dannenberg, J. J.; Rios, R. Theoretical study of the enolic forms of acetylacetone - How strong is the H-bond, *J. Phys. Chem*. **1994**, *98*, 6714-6718.

(80) Yoon, M. C.; Choi, Y. S.; Kim, S.K. The OH production from the π-π* transition of acetylacetone, *Chem. Phys. Lett*. **1999**, *300*, 207-212.

(81) Nakanishi, H.; Morita, H.; Nagakura, S. Electronic structure and spectra of the keto and enol forms of acetylacetone, *Bull. Chem. Soc. Jap.* **1977**, *50*, 2255-2261.

(82) Zhou, S.; Barnes, I.; Zhu, T.; Bejan, I.; Albu, M. ; Benter Th. Atmospheric Chemistry of Acetylacetone, *Environ. Sci. Technol.* **2008,** *42,* 7905-7910.

(83) Paulot, F.; Crounse, J. D.; Kjaergaard, H. G.; Kroll, J. H.; Seinfeld, J. H.; Wennberg, P. O. Isoprene photooxidation: new insights into the production of acids and organic nitrates, *Atmos. Chem. Phys.* **2009**, *9*, 1479-1501.

(84) Müller, J.-F.; Peeters, J.; Stavrakou, T. Fast photolysis of carbonyl nitrates from isoprene, *Atmos. Chem. Phys*. **2014**, *14*, 2497-2508.

(85) Crounse, J.D.; Knap, H. C.; Ørnsø, K. B.; Jørgensen, S.; Paulot F.; Kjaergaard, H. G.; Wennberg, P. O. Atmospheric Fate of Methacrolein. 1. Peroxy Radical Isomerization Following Addition of OH and O_2, *J. Phys. Chem. A* **2012**, *116*, 5756-5762.

(86) Méreau, R.; Rayez, M. T.; Rayez J. C. ; Caralp, F.; Lesclaux, R. Theoretical study on the atmospheric fate of carbonyl radicals :kinetics of decomposition reactions, *Phys. Chem. Chem. Phys*. **2001**, *3*, 4712-4717.

(87) Hasson, H. S.; Tyndall, G. S.; Orlando, J. J. A product yield study of the reaction of HO_2 radicals with ethyl peroxy ($C_2H_5O_2$), acetyl peroxy ($CH_3C(O)O_2$) and acetonyl peroxy ($CH_3C(O)CH_2O_2$) radicals, *J. Phys. Chem. A* **2004**, *108*, 5979-5989

(88) Crounse, J. D.; Paulot, F.; Kjaergaard, H. G.; Wennberg, P. O. Additions and Corrections to Peroxy radical isomerization in the oxidation of isoprene, *Phys. Chem. Chem. Phys.* **2011**, *13*, 13607-13613", ***Amendment published 6th September 2012***

(89) Leu, G.-H.; Huang, C.-L.; Lee, S.-H.; Lee, Y.-C.; Chen, I.-C. Vibrational levels of the transition state and rate of dissociation of triplet acetaldehyde, *J. Chem. Phys*. **1998**, *109*, 9340-9350.

(90) A. Novelli[1], K. Hens[1], C. Tatum Ernest[1], D. Kubistin[1,*], E. Regelin[1], T. Elste[2], C. Plass-Dülmer[2], M. Martinez[1], J. Lelieveld[1], and H. Harder[1] Characterisation of an inlet

pre-injector laser induced fluorescence instrument for the measurement of ambient hydroxyl radicals, *Atmos. Meas. Tech. Discuss.*, **2014**, 7, 819-858.

Table of Contents (TOC) Image

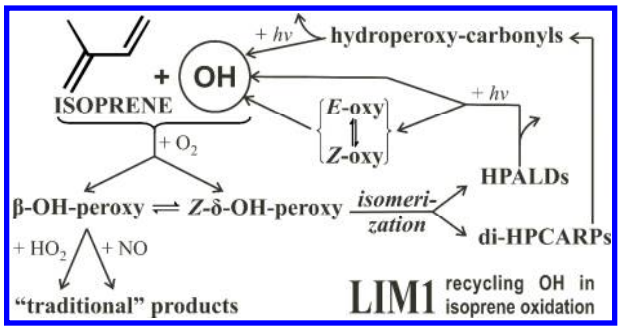

Table of Contents (TOC) Graphic